

Journal Pre-proof

A Covalent p97/VCP ATPase Inhibitor can overcome resistance to CB-5083 and NMS-873 in colorectal cancer cells

Gang Zhang, Shan Li, Feng Wang, Amanda C. Jones, Alexander F.G. Goldberg, Benjamin Lin, Scott Virgil, Brian M. Stoltz, Raymond J. Deshaies, Tsui-Fen Chou



PII: S0223-5234(20)31120-X

DOI: <https://doi.org/10.1016/j.ejmech.2020.113148>

Reference: EJMECH 113148

To appear in: *European Journal of Medicinal Chemistry*

Received Date: 22 November 2020

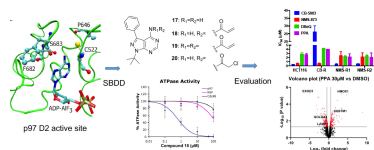
Revised Date: 16 December 2020

Accepted Date: 28 December 2020

Please cite this article as: G. Zhang, S. Li, F. Wang, A.C. Jones, A.F.G. Goldberg, B. Lin, S. Virgil, B.M. Stoltz, R.J. Deshaies, T.-F. Chou, A Covalent p97/VCP ATPase Inhibitor can overcome resistance to CB-5083 and NMS-873 in colorectal cancer cells, *European Journal of Medicinal Chemistry*, <https://doi.org/10.1016/j.ejmech.2020.113148>.

This is a PDF file of an article that has undergone enhancements after acceptance, such as the addition of a cover page and metadata, and formatting for readability, but it is not yet the definitive version of record. This version will undergo additional copyediting, typesetting and review before it is published in its final form, but we are providing this version to give early visibility of the article. Please note that, during the production process, errors may be discovered which could affect the content, and all legal disclaimers that apply to the journal pertain.

© 2021 Elsevier Masson SAS. All rights reserved.



Journal Pre-proof

A Covalent p97/VCP ATPase Inhibitor can overcome resistance to CB-5083 and NMS-873 in colorectal cancer cells

Gang Zhang^{a,#}, Shan Li^{a,#}, Feng Wang^{a,#}, Amanda C. Jones^{b,#,\$}, ~~Hosea Nelson^b~~, Alexander F. G. Goldberg^b, ~~Kimberly Petersen^b~~, ~~Joshua Owen^b~~, ~~Anguel Alexiev^b~~, Benjamin Lin^b, ~~Jonny Gordon^b~~, Scott Virgil^b, Brian M. Stoltz^{b,*}, Raymond J. Deshaies^{a,c,%*} and Tsui-Fen Chou^{a,d,*}

^a*Division of Biology and Biological Engineering, California Institute of Technology, Pasadena, CA 91125, United States*

^b*Division of Chemistry and Chemical Engineering, California Institute of Technology, Pasadena, CA 91125, United States*

^c*Howard Hughes Medical Institute, Chevy Chase, MD 20815, United States*

^d*Proteome Exploration Laboratory, Beckman Institute, California Institute of Technology, Pasadena, CA 91125, United States*

[#]These authors made equal contributions to this work.

Current Address:

^{\$} Department of Chemistry, Box 7486, Wake Forest University

[%] Amgen Research, Thousand Oaks, CA, USA.

*Corresponding authors. Tel.: +1 626-395-6772 (Tsui-Fen Chou), +1 626-395-6064 (Brian M. Stoltz).
Email addresses: tfchou@caltech.edu (Tsui-Fen Chou), rdii2003@gmail.com (Raymond J. Deshaies), stoltz@caltech.edu (Brian M. Stoltz)

Abstract

Small-molecule inhibitors of p97 are useful tools to study p97 function. Human p97 is an important AAA ATPase due to its diverse cellular functions and implication in mediating the turnover of proteins involved in tumorigenesis and virus infections. Multiple p97 inhibitors identified from previous high-throughput screening studies are thiol-reactive compounds targeting Cys522 in the D2 ATP-binding domain. Thus, these findings suggest a potential strategy to develop covalent p97 inhibitors. We first used purified p97 to assay several known covalent kinase inhibitors to determine if they can inhibit ATPase activity. We evaluated their selectivity using our dual reporter cells that can distinguish p97 dependent and independent degradation. We selected a β -nitrostyrene scaffold to further study the structure-activity relationship. In addition, we used p97 structures to design and synthesize analogues of pyrazolo[3,4-*d*]pyrimidine (PP). We incorporated electrophiles into a PP-like compound **17** (4-amino-1-*tert*-butyl-3-phenyl pyrazolo[3,4-*d*]pyrimidine) to generate eight compounds. A selective compound **18** (*N*-(1-(*tert*-butyl)-3-phenyl-1*H*-pyrazolo[3,4-*d*]pyrimidin-4-yl)acrylamide, **PPA**) exhibited excellent selectivity in an *in vitro* ATPase activity assay: IC₅₀ of 0.6 μ M, 300 μ M, and 100 μ M for wild type p97, yeast Cdc48, and N-ethylmaleimide sensitive factor (NSF), respectively. To further examine the importance of Cys522 on the active site pocket during PPA inhibition, C522A and C522T mutants of p97 were purified and shown to increase IC₅₀ values by 100-fold, whereas replacement of Thr532 of yeast Cdc48 with Cysteine decreased the IC₅₀ by 10-fold. The molecular modeling suggested the hydrogen bonds and hydrophobic interactions in addition to the covalent bonding at Cys522 between WT-p97 and PPA. Furthermore, tandem mass spectrometry confirmed formation of a covalent bond between Cys522 and PPA. An anti-proliferation assay indicated that the proliferation of HCT116, HeLa, and RPMI8226 was inhibited by PPA with IC₅₀ of 2.7 μ M, 6.1 μ M, and 3.4 μ M, respectively. In addition, PPA is able to inhibit proliferation of two HCT116 cell lines that are resistant to CB-5083 and NMS-873, respectively. Proteomic analysis of PPA-treated HCT116 revealed Gene Ontology enrichment of known p97 functional pathways such as the protein ubiquitination and the ER to Golgi transport vesicle membrane. In conclusion, we have identified and characterized PPA as a selective covalent p97 inhibitor, which will allow future exploration to improve the potency of p97 inhibitors with different mechanisms of action.

KEY WORDS

P97; Covalent inhibitor; ATPase Activity; Organic Synthesis; Docking; Anti-proliferative activity; Proteomics

1. Introduction

ATPases associated with diverse cellular activities (AAA+ proteins) are enzymes sharing a common conserved module of approximately 230 amino acid residues [1] and are functionally diverse protein families belonging to the AAA+ protein superfamily of ring-shaped P-loop NTPases. AAA+ proteins catalyze the hydrolysis of a phosphate bond in adenosine triphosphate (ATP), releasing adenosine diphosphate (ADP), inorganic phosphate, and energy to facilitate a variety of cellular processes that are essential for life, including protein folding [2], intracellular transport [3], protein degradation [4], initiation of DNA replication [5], DNA repair [6], DNA remodeling [7], and ion transport [8].

p97, also known as valosin-containing protein (VCP) and Cdc48 (cell division cycle protein 48) in *Saccharomyces cerevisiae*, Ter94 (transitional endoplasmic reticulum ATPase) in *Drosophila melanogaster* and VAT (VCP-like ATPase) in *Thermoplasma acidophilum*, is a hexameric type II AAA+ ATPase. p97 is involved in a wide range of cellular functions, including endoplasmic reticulum-associated degradation (ERAD), membrane fusion, nuclear factor kappa-light-chain-enhancer of activated B cells (NF- κ B) activation, and chromatin-associated processes, which are regulated by ubiquitination. [9] p97 consists of two AAA ATPase domains in tandem, D1, and D2, respectively. A short polypeptide linker (D1-D2 linker) connects the two ATPase domains while the N-D1 linker joins the D1 domain to a large amino-terminal domain (N-domain). The carboxyl-terminus of the D2 domain features a short tail containing ~40 residues. Interaction of p97/Cdc48 with its partners is mostly mediated by the N-domain, although a few proteins bind p97/Cdc48p via the C terminus [10, 11]. Both D1 and D2 domains are homologous in sequence and in structure [12]. The D1 domain has lower intrinsic ATPase activity than does the D2 domain [13], while the D2 domain was thought to underlie p97 function as a mechanochemical transducer, which contributed most of the ATPase activity [14]. Protein substrates released by p97 can be degraded by the 26S proteasome [15, 16]. In addition, p97 is involved in another form of protein degradation and recycling, namely autophagy [17]. The expression levels of p97 are upregulated in many cancers, such as colorectal cancer, pancreatic cancer, thyroid cancer, squamous cell carcinoma, breast cancer, osteosarcoma, gastric carcinoma, and lung cancer [18]. Therefore, p97 is considered a potential anticancer target.

Currently, there are several p97 inhibitors reported (**Fig. 1**), classified as either ATP-competitive or allosteric inhibitors. The ATP-competitive inhibitor DBEq (N^2, N^4 -Dibenzylquinazoline-2,4-diamine) mainly targets the D2 domain. DBEq blocks many biological processes, including degradation of ubiquitin-fusion degradation and ERAD pathway substrates, as well as autophagosome maturation [19-21]. Two DBEq derivatives with IC_{50} values of ~100 nM, ML240 and ML241, have been developed. ML240 stimulates the accumulation of LC3-II and rapidly mobilizes the executioner caspases 3 and 7. ML240 also has broad antiproliferative activity toward the NCI-60 panel of cancer cell lines and synergizes with the proteasome inhibitor MG132 to kill multiple colon cancer cell lines. Both ML240 and ML241 have low off-target activity toward a panel of protein kinases and central nervous system targets. [22] CB-5083, derived by structure-activity relationship of the ML240 scaffold, is a selective, ATP-competitive, and orally bioavailable p97 inhibitor, which activates the apoptotic arm of the unfolded protein response and exhibits antitumor activity in several hematological and solid tumor models. CB-5083 entered phase I clinical trials for multiple myeloma in 2015 [23, 24]. However, the trial was terminated due to toxicity caused by an off-target effect. Its successor CB-5339, as the second-generation clinical-grade inhibitor of p97, is in phase I clinical trials for Acute Myeloid Leukemia or Myelodysplastic Syndrome [25]. One of the major challenges of targeted cancer therapy is the emergence of drug-resistant mutations in tumor cells leading to loss of treatment effectiveness. Mutations in p97 that cause resistance to CB-5083 have been identified [23]. Availability of different p97 inhibitors with various binding modes may help overcome this issue. Recently, LC-1028 was reported as a covalent p97 inhibitor with a Michael acceptor consisting of a carbonyl group conjugated with a methyl-capped acetylene group [26]. LC-1028 showed antiproliferative activity in MIA PaCa-2 cells with an EC_{50} value of 0.436 μ M. LC-MS/MS suggested LC-1028 conjugates to C522, indicating that LC-1028 binds to the

D2 domain by a covalent bond; the docking model was consistent with this result. However, the selectivity of LC-1028 against WT-p97 over other AAA+ ATPases remains unclear. Although there is a much research on the inhibition of p97 and clinical trials are ongoing to evaluate CB-5339, no drug has been approved by the FDA to target p97.

Nerviano Medical Sciences and Genentech discovered the allosteric inhibitor NMS-873, an alkylsulfanyl-1,2,4-triazole analog that binds in a tunnel between the D1 and D2 domains [27, 28]. NMS-873 inhibited the ERAD pathway and led to the accumulation of misfolded proteins in the ER. [29] UPCDC30245 is another allosteric p97 inhibitor with an IC_{50} of 27 nM, which reversibly binds at the interface of the D1 and D2 domains as determined by cryo-electron microscopy [30]. Eeyarestatin I (EerI) serves as a prodrug to convert the 5-nitrofuranyl (NFC) group into a reactive metabolite involved in inhibition of p97-dependent protein degradation in cells even though the exact mechanism of the active metabolite still remains unknown [31, 32]. NMS-859 is a covalent p97 inhibitor, featuring an electrophilic α -chloroacetamide, which selectively modifies Cys522 in the D2 active site with an IC_{50} of 0.37 μ M [28].

MSC1094308 [33] and 2-aminopyridine indole amide [34] are reported as two allosteric p97 inhibitors with IC_{50} values of 7.2 μ M and 0.5 μ M, respectively. MSC1094308, with low biochemical potency, showed cellular efficacy at 10 μ M. The 2-aminopyridine indole amide exhibited excellent physicochemical properties, including solubility (330 μ M in PBS), bidirectional permeability (710 and 460 nm/s), and microsomal stability (human $T_{1/2}$ > 60 min). $\Delta(10,11)$ -Dehydrocurvularin [35] and Withaferin A 27-Acetate [36] covalently modify p97. $\Delta(10,11)$ -Dehydrocurvularin inhibited p97 with an IC_{50} value of 15.3 ± 9.9 μ M by covalent bond with Cys522 of p97. Withaferin A 27-Acetate exhibited inhibitory activity against wild-type p97 with an IC_{50} value of 21 μ M, but it didn't show inhibition against the C522A mutant. However, Withaferin A 27-Acetate exhibited anti-proliferative effects in cancer cell lines at 10-fold lower concentration, suggesting additional modes of action. Clotrimazole [37], Oxaspirol B [38], and 5'-I-Fuligocandin B [39] exhibited p97 inhibition activity with IC_{50} values of 12 μ M, 31.2 ± 3.0 μ M and 7.0 μ M, respectively. However, their mechanisms of action are unclear. Herein, we report the design, optimization, and biological evaluation of a covalent p97 inhibitor with the potential to be a specific and useful tool to uncover p97's function and to be further developed to treat cancers.

2. Results and Discussion

2.1 Search for potential irreversible kinase inhibitors to inhibit p97 *in vitro* and in cells

High throughput (HTS) screens identified multiple hits containing electrophilic groups with sub-micromolar IC_{50} values for inhibiting ATPase activity of purified p97 *in vitro* and turnover of a p97-dependent cellular reporter [21]. C522A p97 is less sensitive to these electrophilic compounds [21, 40]. One of the hits, an aryl alkynyl ketone (Compound **1**, JFD02342), inhibited ATPase activity with IC_{50} of 0.2 μ M. However, it also inhibited the turnover of both p97-dependent (Ub^{G76V}-GFP) and independent reporters (ODD-Luc) (**Table 1**). To search for irreversible p97 inhibitors, we evaluated several characterized kinase inhibitors with our *in vitro* and cell-based p97 HTS assays [41]. Compound **2** is a spleen tyrosine kinase (Syk) inhibitor [42, 43], compounds **4** (cmk), and **5** (fmk) are halomethylketone pyrrolopyrimidine-based p90 ribosomal protein S6 kinase (RSK) inhibitors [44], and compound **6** is a 6-acrylamido-4-anilinoquinazoline-based inhibitor against epidermal growth factor receptor (EGFR) [45]. Compounds **1-3** demonstrated submicromolar IC_{50} , compound **5** was 10-fold less active than the corresponding chloro-substituted compound **4**, and compound **6** exhibited IC_{50} values about 10-18 μ M (**Table 1**). Compound **2** (3,4-methylenedioxy- β -nitrostyrene) [41] was chosen for more detail analysis due to its lower IC_{50} values in both *in vitro* ATPase and in cell Ub^{G76V}-GFP degradation assays.

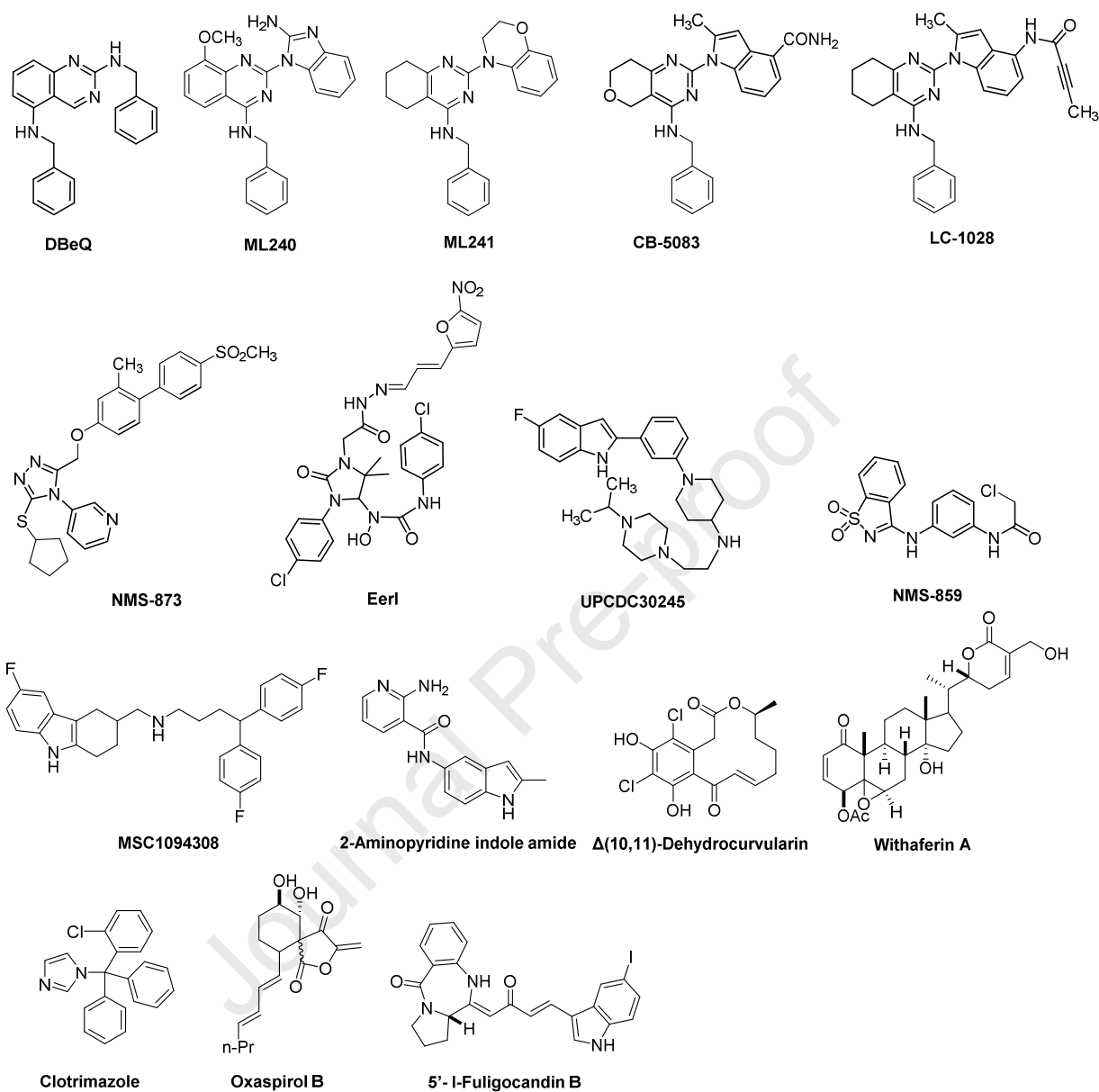
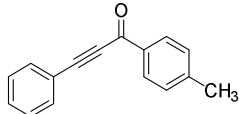
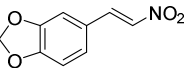
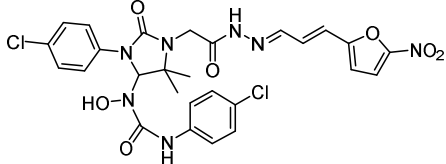
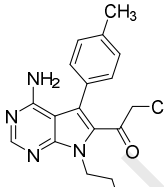
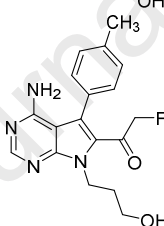
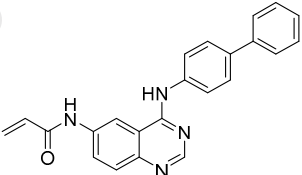


Figure. 1 Chemical Structure of Known p71 Inhibitors

Table 1 Apparent IC₅₀ values of known irreversible inhibitors against p97 and its reporters

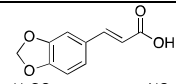
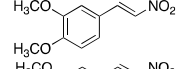
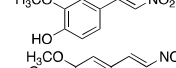
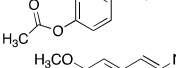
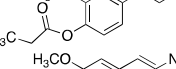
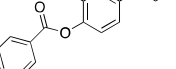
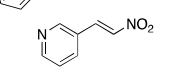
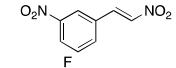
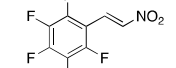
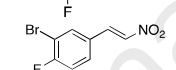
Compounds	Structures	Apparent IC ₅₀ (μM) ^a		
		Ub ^{G76V} -GFP	ODD-Luc	p97
1^b (JFD02342)		3.4 ± 1.0	5.2 ± 1.8	0.2 ± 0.02
2^b (β-nitrostyrene)		1.6 ± 0.4	3.9 ± 1.0	1.7 ± 0.5
3 (EerI)		3.7 ± 0.4	ND ^c	> 30
4 (cmk)		5.8 ± 1.1	4 ± 2	3.9 ± 0.9
5 (fmk)		47 ± 10	39 ± 3	> 30
6		18 ± 4	11 ± 5	10 ± 5

^a Measurements were carried out in triplicate, and variance is expressed as the standard deviation.

^b Data for compounds 1 and 2 were adapted from references [21] and [41], respectively.

^c ND: Not Determined

Table 2 Apparent IC₅₀ values of compound 2 analogs against p97 and its reporters

Compounds	Structures	Apparent IC ₅₀ (μM)		
		Ub ^{G76V} -GFP	ODD-Luc	p97
7		> 30	> 30	>30
8		1.9 ± 0.9	1.8 ± 0.9	3.1 ± 1.8
9		6.8 ± 2.5	5 ± 0.8	13 ± 5
10		5.7 ± 1.5	2.3 ± 0.9	3.6 ± 2.8
11		4.3 ± 1.6	1.6 ± 0.8	3.4 ± 1.8
12		5.7 ± 2.8	10 ± 3	2.0 ± 0.4
13		2.9 ± 0.7	3.0 ± 1.0	0.7 ± 0.3
14		1.7 ± 0.7	4.0 ± 1.4	1.2 ± 0.3
15		2.7 ± 1.0	2.1 ± 0.3	2.4 ± 0.6
16		1.8 ± 0.8	2.0 ± 0.9	1.7 ± 0.5

To examine structure-activity relationships of the β-nitrostyrene scaffold, we obtained five and prepared five analogues (compounds **7-16**, **Table 2**). Replacing the nitro group with carboxylic acid (compound **7**) led to complete loss of activity, therefore suggesting the nitro group is critical for the observed inhibition. The only other modification that affected both assays by more than 3-fold was the placement of a hydroxyl group in *para*-substitution to the nitro styrene moiety (compound **9**). The requirement for the nitro group and the relative insensitivity of the remainder of the scaffold to modification suggested that the primary mechanism of action was a covalent reaction with Cys522 in the D2 domain active site. The poor activity of Compound **2** towards the C522A mutant and its sensitivity to DTT indicated that the electrophilic attack of Cys522 was indeed critical for the potency of Compound **2**. [41] Compound **2** was first reported to be a selective Syk inhibitor [43] with submicromolar IC₅₀; however, our results indicated that it is a potent p97 inhibitor *in vitro* and in cells, but we were unable to obtain a selective analogue for inhibiting p97 in cells, which is likely due to the high reactivity of the electrophilic moiety. We then sought to design an irreversible scaffold by using x-ray crystal structures of p97 (PDB code 1e32).

2.2 Structure based drug design to develop a covalent inhibitor of p97

To develop covalent inhibitors of p97, we focused our attention on the D2 ATPase domain. This domain has a cysteine residue at position 522, the side chain of which projects into the active site nearby the amino group (NH₂) attached at the C6 position of the purine of a bound ADP-aluminum fluoride complex (**Fig. S1a**) [46]. We reasoned that an ATP analog carrying an electrophilic substitution at C6 might react with this cysteine residue and inactivate p97. It is noteworthy that a cysteine at position 522 is

not essential for p97 ATPase activity, and in fact the budding yeast ortholog of p97, Cdc48, does not have cysteine in this position. Indeed, the presence of cysteine at this position in members of the AAA ATPase family is variable: the D1 domain of NSF has a cysteine in the equivalent position, whereas five of the six AAA ATPase subunits of the 26S proteasome do not (**Fig. S1b**). To develop an inhibitor capable of reacting with this cysteine, we selected PP (compound **17**) as the starting point and optimized this scaffold in a variety of ways in terms of the binding mode of the Src inhibitor pyrazolopyrimidines (PPs) (**Fig. 2**) [47, 48]. Specifically, we attached various electrophilic groups to the C4 position, including acrylamides (compounds **18**, **19**, **22**, **23**, **24**, **27**, and **28**), and a chloroacetamide (compound **20**). As negative controls, we prepared compounds that retained an amino group attached at C4 (compounds **17**, **21**, **25**, and **26**). All compounds demonstrated inhibitory activity in both ATPase and Ub^{G76V}-GFP turnover assays except for the control compounds (**Table 3**). The most potent inhibitor was compound **18** (PPA), which contains benzene at C3 and a single acrylamide at C4. PPA was 20-fold less potent at inhibiting the p97-independent reporter. Therefore, we selected PPA for a more detailed study.

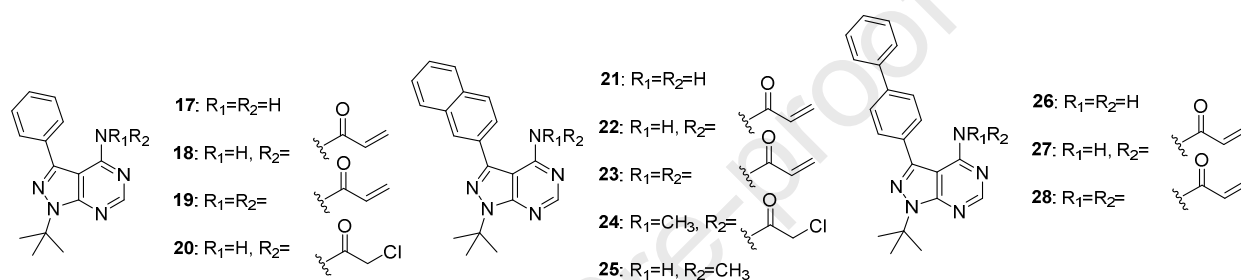


Figure. 2 Structures of the pyrazolo[3,4-*d*]pyrimidine analogs designed for p97 inhibition.

Table 3 Apparent IC₅₀ values of the pyrazolo[3,4-*d*]pyrimidine analogs against p97, T532C-Cdc48, and the cellular reporters.

Compounds	Apparent IC ₅₀ (μM)*			
	Ub ^{G76V} -GFP	ODD-Luc	p97	T532C-Cdc48
17	> 30	> 30	> 100	> 100
18 (PPA)	1.6 ± 0.5	35 ± 10	0.6 ± 0.2	14 ± 5
19	5.4 ± 1.6	> 30	1.1 ± 0.7	26 ± 6
20	31 ± 3	> 30	4.5 ± 3.5	35 ± 8
21	> 30	> 30	> 100	> 100
22	2.0 ± 0.9	> 30	3 ± 1	24 ± 7
23	2.5 ± 0.3	> 30	1.3 ± 0.7	22 ± 11
24	3.6 ± 0.5	> 30	10 ± 6	ND
25	> 30	> 30	> 50	ND
26	> 30	> 30	> 50	ND
27	2.1 ± 0.6	> 30	2.8 ± 1.2	ND
28	6.1 ± 0.7	> 30	0.9 ± 0.2	ND

*Measurements were carried out in triplicate, and variance is expressed as the standard deviation. ND: not determined.

2.3 Biochemical characterization of PPA (18)

To determine if inhibition by PPA requires a reactive thiol, we determined inhibition of ATPase activity in the presence of dithiothreitol (DTT) and cysteine during the preincubation. The data in **Figure S1c** demonstrated that the inhibitory effect of PPA could be counteracted by the inclusion of either cysteine or DTT. To evaluate whether PPA modifies cysteine 522, inhibited p97 was digested with trypsin, and peptides were fractionated by HPLC and analyzed by tandem mass spectrometry. The PPA-modified peptide (N14) from the digested p97 sample was eluted using PPA-modified N15-labeled peptide ($\text{H}_2\text{N-GVLFYGP}^*\text{P}^*\text{GCGK-OH}$, where * indicates N15 labeled residues) as an internal control (**Fig. S2**). Tandem mass spectrometry identified Cys522 as the site of modification, thus confirming the formation of a covalent bond between PPA and p97. To further address whether Cys522 is necessary for inhibition of p97 by PPA, we constructed two mutants in which Cys522 was converted to either alanine or threonine. Furthermore, we constructed a mutant of yeast Cdc48 in which the residue analogous to Cys522, Thr532, was converted to cysteine. Mutation of Cys522 in p97 to either alanine or threonine decreased sensitivity to PPA by more than 100-fold (**Table 4**). On the other hand, yeast Cdc48, which normally is quite resistant to PPA, became nearly 30-fold more sensitive to the compound upon the introduction of cysteine in place of Thr532. Together, these data indicate that Cys522 is both necessary and sufficient to confer sensitivity to PPA.

Table 4 Cys522-mediated p97 inhibition by PPA (18) *in vitro*

Enzyme	Apparent IC_{50} (μM)
WT-p97	0.62 ± 0.25
C522A-p97	110 ± 33
C522T-p97	82 ± 45
Yeast Cdc48	376 ± 95
T532C-yeast Cdc48	14 ± 5
Hamster NSF	105 ± 31
Human 19S ATPase*	75 ± 19

*Human Rpt3 contains a cysteine in Walker A motif.

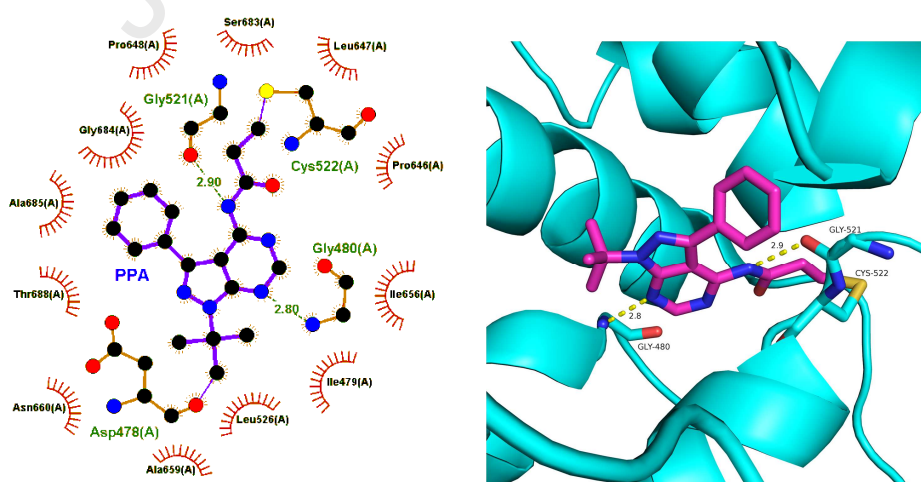


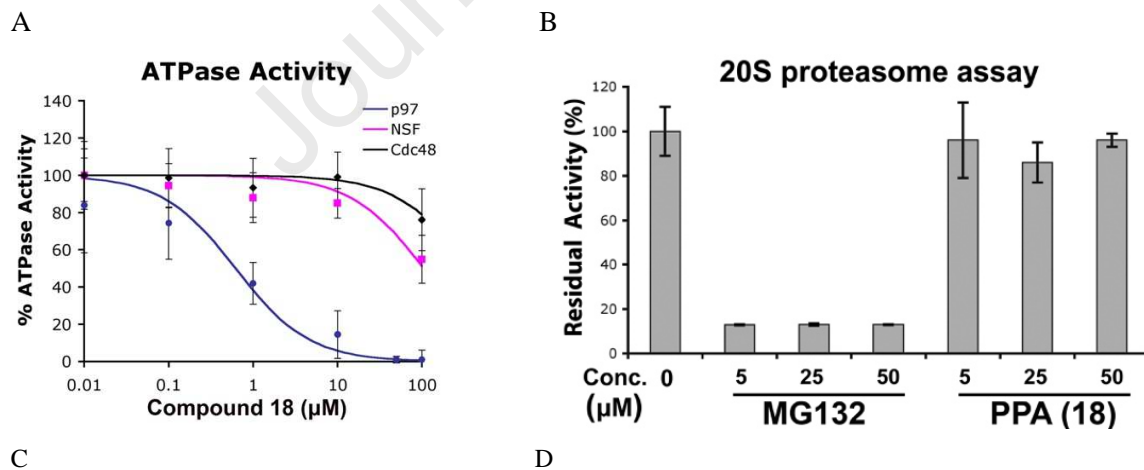
Figure. 3 The docking study of PPA into WT-p97. (A) Two-dimensional presentation of the potential interactions between PPA and WT-p97. (B) Three-dimensional presentation of PPA in the active site.

2.4 Docking study of PPA (18)

Although we have confirmed the covalent binding of PPA to Cys522 in Domain 2, it is still unclear whether other interactions between PPA and WT-p97 occur. In order to understand the binding mode of PPA in the active site, we performed the covalent docking study by AutoDock 4.2.6. [49] In addition to the covalent bonding to Cys522 between the terminal carbon atom from the acryl amido group and the thiol group, there were two hydrogen bond interactions between Gly480 and 7-NH, and Gly521 and the amido NH, respectively (**Fig. 3A and 3B**). In addition, some residues in the active site, such as Ile479, Leu526, Gly684, Ala685, and Thr688 showed hydrophobic interactions with PPA (**Fig. 3A**).

2.5 PPA does not inhibit NSF and 26S proteasome and blocks degradation of p97 substrate irreversibly

To further address the specificity of PPA, we tested its activity against two other AAA ATPases, NSF, and the 19S regulatory particles. Although NSF is known to be sensitive to thiol-reactive agents, it was more than 100-fold less sensitive to PPA than p97 (**Fig. 4A, Table 4**). Likewise, inhibition of ATP hydrolysis by the 19S regulatory particles was observed only at high concentrations of PPA ($IC_{50} = 75 \mu M$). The results with NSF and the 19S regulatory particles are noteworthy because both the active D1 domain of NSF and the Rpt3 subunit of the 19S regulatory particles have cysteine in the position analogous to cysteine 522 of p97 (**Fig. S1b**). Moreover, PPA did not inhibit the hydrolysis of a fluorogenic proteasome substrate, LLVY-AMC, with the affinity-purified 26S proteasome from Hek293 cells [50] (**Fig. 4B**). We used previously established washout assay using Ub^{G76V}-GFP reporter to demonstrate PPA irreversibly block degradation of Ub^{G76V}-GFP in cells [41]. Ub^{G76V}-GFP was degraded after washing out MG132 but it remains stable with PPA treated cells (**Fig. 4C**). Similarly, we showed that PPA block degradation of an ERAD substrate, TCR α -GFP (α -chain of the T-cell receptor fused to GFP) [51]. We included MG132 (a reversible proteasome inhibitor), YU101 (a covalent proteasome inhibitor) [52], PYR41 (a ubiquitin E1 inhibitor) [53], and DBeQ (a reversible p97 inhibitor) [21] as positive controls.



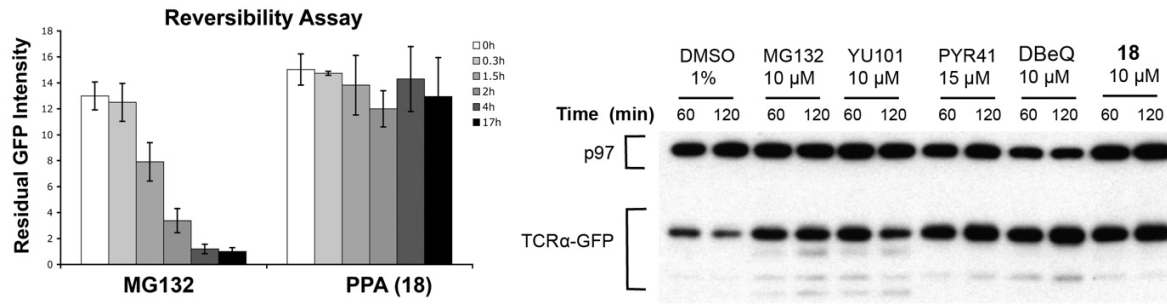


Figure 4. PPA inhibits p97 ATPase activity selectively and irreversibly. (A) Titration curves of the *in vitro* ATPase assays for PPA inhibition of p97, NSF, and Cdc48. (B) PPA did not inhibit human 26S proteasome activity. (C) Reversibility of PPA inhibition was determined using Ub^{G76V}-GFP by washing out test compound and monitoring decay of GFP signal in the presence of cycloheximide for additional 17 h. (D) PPA block degradation of an ERAD substrate, TCRα-GFP stably expressed in HEK293 cells. Cells were incubated with MG132, washed and treated with cycloheximide plus compound for 60 min or 120 min. Samples were immunoblotted with anti-p97 as loading control and anti-GFP antibody to detect TCRα-GFP.

2.6 Anti-proliferative effect of PPA in cancer cells and in CB-5083, NMS-873 resistant colorectal cancer

To explore anti-proliferative effects of these compounds, we used three cancer cell lines and evaluated PPA together with three known p97 inhibitors, CB-5083, NMS-873, and DBEIQ. As shown in **Fig. 5A**, all compounds inhibited proliferation of all three cancer lines. CB-5083 showed the most potent anti-proliferative activity. The IC₅₀ of PPA to HCT116, HeLa, and RPMI8226 were 2.7 μM, 6.1 μM, and 3.4 μM respectively. PPA has comparable potency as DBEIQ and less potent compared to CB-5083 and NMS-873. PPA's cellular activity was consistent with its enzymatic activity against p97. Furthermore, we evaluated its potency toward CB-5083 resistant (CB-R) and NMS-873 resistant (NMS-R) HCT116 cell lines [24], as shown in **Fig. 5B**, PPA and DBEIQ have similar anti-proliferative activities for all three HCT116 lines. CB-5083 is 72-fold less effective in CB-R, whereas NMS-873 is 4.5-fold less effective in NMS-R. The two NMS-873 resistant cell lines we isolated are A530T heterozygous, so the fold resistance is not as high as the homozygous A530T made using CRISPR as described previously [54].

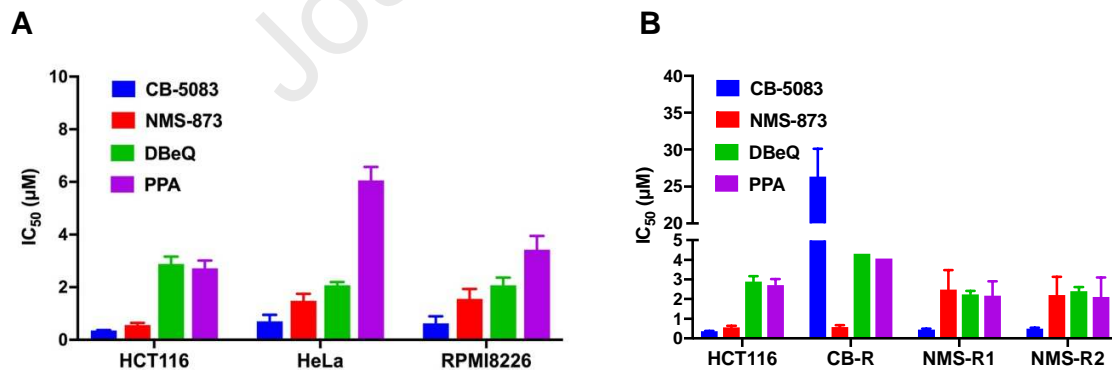


Figure 5. Anti-proliferation activity of p97 inhibitors against (A) HCT116, HeLa, and RPMI8226 cell lines. (B) HCT116, CB-5083 resistant HCT116 cell line harboring D649A, T688A p97 mutant (CB-R) and NMS-873 resistant HCT116 cell line harboring A530T p97 mutant (NMS-R). Data are shown as Mean ± SEM taken from four replicate experiments.

2.7 Quantitative Proteomic Analysis of PPA treated HCT116 human colon cancer cells

Label-free quantification using the Orbitrap Eclipse LC-MS/MS was employed to evaluate the effect of PPA (15 μM or 30 μM for 6 hours) on the protein level changes in HCT116 cells. Two independent

biological replicates were performed for each group. The proteome analysis using PD 2.4 software identified a total of 5924 proteins from all control and PPA-treated groups. The normalized abundance was used for the following analysis (**Fig. S3**). We identified 291 proteins change in 15 μM PPA-treated samples (**Fig. 6A**), and 553 proteins change in 30 μM PPA-treated samples (**Fig. 6B** and **7A**) by limma analysis ($p < 0.05$). The Venn diagram shows that the level of 58 proteins significantly increased (**Fig. 6C**, **Table S3A**) and 46 significantly decreased (**Fig. 6D**, **Table S3B**) in both treatment groups. By overlapping with known p97 interaction data from BioGRID database, we found 33 of them significantly increased (**Fig. 6C**) and 42 of them significantly decreased (**Fig. 6D**) in either 15 or 30 μM treatment groups. Notably, there are 15 known p97 interacting proteins also showed differentially change in both treatment groups and the log₂ fold change values are shown in **Table 5**. For example, SQSTM1 (also known as p62) [55], a ubiquitin binding protein involved in autophagy, antioxidant response, apoptosis, and regulation of endosomal trafficking, is increased in a concentration-dependent manner (logFC 0.42 vs 0.97, 15 μM vs 30 μM). Another protein GOLGA3 [56], participating in transport of protein, apoptosis, and positioning of the Golgi, is dose-dependently decreased (logFC -0.36 vs -0.70, 15 μM vs 30 μM). These results provide valuable insights for further investigation into the mechanisms by which PPA affects p97 function.

The 30 μM PPA-treated group had more significantly changed proteins (~2 fold more than 15 μM PPA-treated group), which suggests that this group might be more informative as to PPA induced proteomic changes. Therefore, subsequent analyses compared DMSO and 30 μM PPA-treated groups. A set of 110 proteins identified in this analysis was classified as the final differentially expressed proteins (DEPs) between the control and 30 μM PPA-treated groups (listed in Table S2), with p -value < 0.05 and fold change > 2 (up-regulated) or < 0.5 (down-regulated). Subsequently, the 110 DEPs were uploaded to the DAVID Database, and the annotation enrichment analysis was carried out with the complete human gene set as the background. We investigated the biological process, molecular function, cellular component, and functional pathways in the significantly enriched GO terms. The top fourteen relevant changed biological processes are presented in **Fig. 7B**. The analysis showed these DEPs are primarily related to protein binding, DNA binding and damage response, and mitochondrion. Some p97-related processes, such as protein ubiquitination and ER to Golgi transport vesicle membrane, were also identified, with other processes linked to PPA's anti-proliferation activity, such as p53 regulation, cell proliferation, and negative regulation of apoptosis. Furthermore, protein-protein interaction (PPI) analysis was performed using the STRING database to understand the interactions between these DEPs in response to treatment with PPA in HCT116 cell lines (**Fig. S4**). For all PPI networks, the minimum required interaction score was set at medium confidence (0.400). The PPI networks showed that the DEPs have several interactions among themselves, suggesting these proteins are biologically connected. For example, the protein HMOX significantly up-regulated in both 15 and 30 μM PPA-treated groups, was shown to interact with many proteins, such as KEAP1, MSRA, MKLN1, CDKN1A, and FTH1.

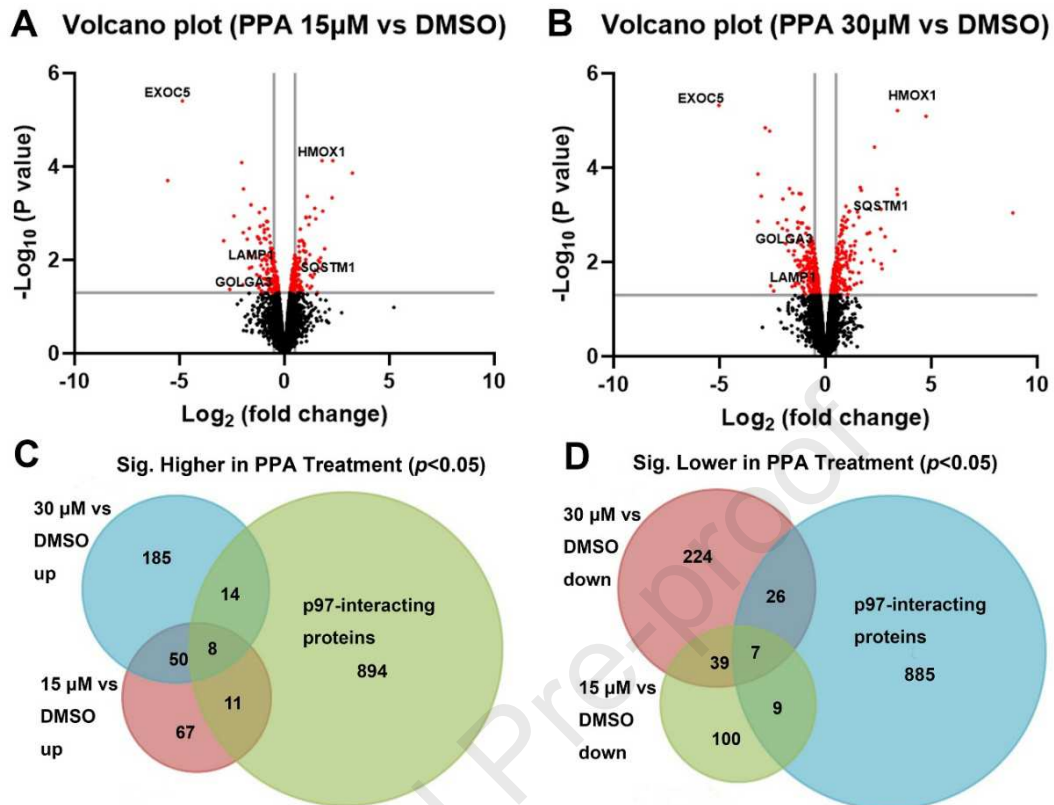


Figure 6 Proteomic analysis of PPA treated HCT116 cell line. A-B) Volcano plots illustrate significantly differentially expressed protein in 15 μM (A) and 30 μM (B) PPA treated HCT116 cells (fold change: PPA/DMSO). C-D) Venn diagrams of up-regulated protein (C) and down-regulated (D) proteins ($p < 0.05$) between 15 μM, 30 μM PPA-treated groups and p97 interactors. The log₂FC range of 15 μM is -5.56 to -0.26 and 0.26 to 3.24 and the log₂FC range of 30 μM are -5.03 to -0.26 and 0.27 to 8.85.

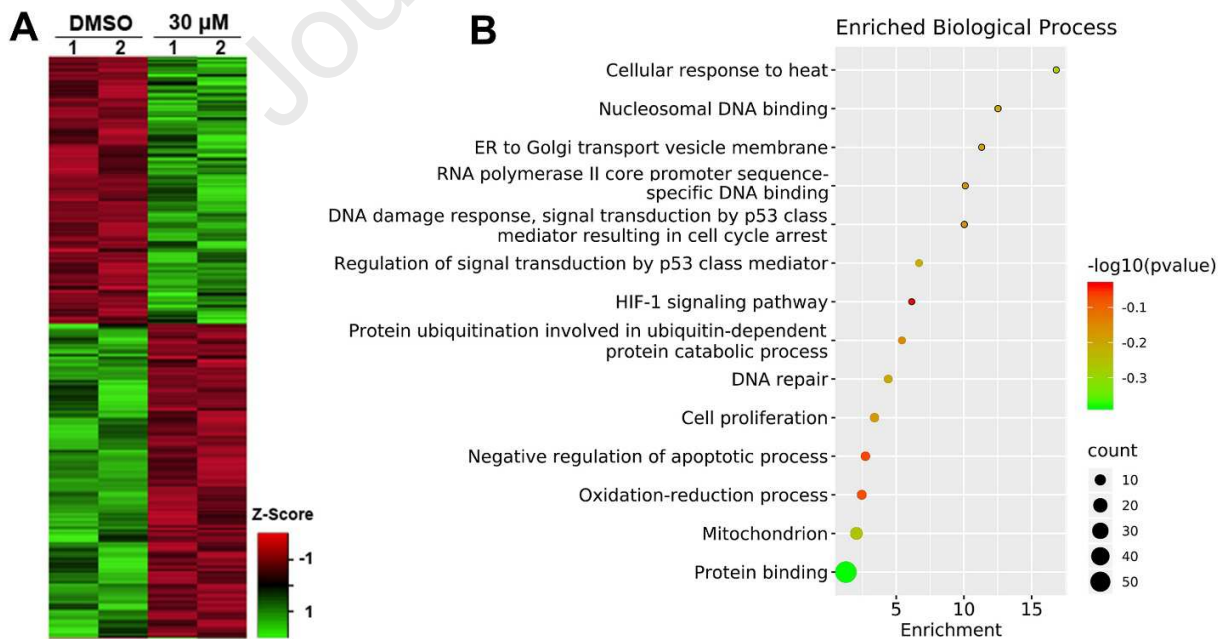


Figure. 7 A) Heatmap presentation of differentially regulated proteins ($p < 0.05$) of DMSO vs. 30 μM PPA-treated groups. B) The biological process analysis of 30 μM PPA-treated group differentially expressed proteins [$p < 0.05$, and $\log_2(\text{FC}) > 1$ or < -1].

Table 5. Overlapped protein list of differentially expressed proteins by 15 μM and 30 μM PPA-treatment known to be regulated by p97. ($p < 0.05$)

Accession	Gene Symbol	Description	log ₂ (Fold Change)	
			15 μM	30 μM
Q15149	PLEC	Isoform 3 of Plectin	0.33	0.58
P58107	EPPK1	Epiplakin	0.38	0.64
Q13501	SQSTM1	Sequestosome-1	0.42	0.97
Q8TCF1	ZFAND1	AN1-type zinc finger protein 1	0.49	0.42
Q8TDN6	BRX1	Ribosome biogenesis protein BRX1 homolog	0.52	0.70
O43422	PRKRIR	52 kDa repressor of the inhibitor of the protein kinase	0.69	0.68
P46736	BRCC3	Lys-63-specific deubiquitinase BRCC36	0.94	0.83
Q13586	STIM1	Stromal interaction molecule 1	1.49	1.65
P11279	LAMP1	Lysosome-associated membrane glycoprotein 1	-0.59	-0.66
O14519	CDK2AP1	Cyclin-dependent kinase 2-associated protein 1	-0.48	-0.47
Q14145	KEAP1	Kelch-like ECH-associated protein 1	-0.46	-1.03
P50748	KNTC1	Kinetochore-associated protein 1	-0.43	-0.87
Q9Y679	AUP1	Ancient ubiquitous protein 1	-0.39	-0.43
Q08378	GOLGA3	Golgin subfamily A member 3	-0.36	-0.70
A0A087WY71	AP2M1	AP-2 complex subunit mu	-0.33	-0.38

3. Conclusion

To develop irreversible p97 inhibitors, we screened six well-characterized kinase inhibitors by our *in vitro* and cell-based p97 HTS assays. Compounds **1** and **2** were chosen to further optimize their structures to provide 10 compounds (compounds **7-16**). Intrigued by the p97 inhibition result of these compounds, we designed and synthesized a series of irreversible p97 inhibitors by introducing a Michael Acceptor on the N-6 position of ADP after analysis of the crystal structure of the p97 complex with ADP-AIF3 (PDB code 1e32). PPA showed potent inhibition against p97 with IC_{50} of $0.6 \pm 0.2 \mu\text{M}$. Its irreversible mode of action was confirmed by tandem mass spectrometry and a washout experiment in a p97 dependent degradation assay. An *in-silico* docking study was performed to validate the feasibility of covalent binding to Cys522. In a panel of Cys522-mediated p97 inhibition assays *in vitro*, PPA showed up to 100-fold selectivity on wild-type vs. Cys522-mutated p97 with IC_{50} of $0.62 \pm 0.25 \mu\text{M}$. In addition, PPA did not show inhibition against NSF and 26S proteasome. In addition, PPA showed potent anti-proliferative effects on HCT116, HeLa, and RPMI8226 cells with IC_{50} values of $2.7 \mu\text{M}$, $6.1 \mu\text{M}$, and $3.4 \mu\text{M}$, respectively. Moreover, PPA can inhibit growth of CB-5083 and NMS-873 resistant HCT116 cells. Furthermore, proteomic analysis revealed PPA regulated bona fide p97 interacting proteins involved in known p97 functional pathways such as protein ubiquitination and ER to Golgi transport vesicle membranes. Taken together, these observations suggest PPA could serve as a promising starting point to develop an irreversible p97 inhibitor to treat cancer and can be a valuable tool to overcome resistance to other p97 inhibitors with different mode of actions such as ATP competitive and allosteric mechanisms.

4. Materials and Methods

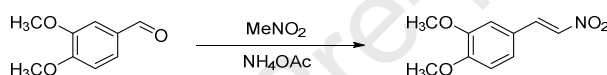
4.1. Chemical Synthesis

4.1.1 Material

Reactions were performed in flame-dried glassware under an argon or nitrogen atmosphere. Solvents were dried by passage through an activated alumina column under argon. Triethylamine (NEt₃) was distilled from sodium hydride immediately prior to use. Other commercial reagents were used as received. Thin-layer chromatography (TLC) was performed using E. Merck silica gel 60 F254 precoated plates (0.25 mm) and visualized by UV fluorescence quenching. Silica *Flash* P60 Academic Silica gel (particle size 0.040-0.063 mm) was used for flash chromatography. ¹H and ¹³C NMR spectra were recorded on either a Varian Mercury 500 spectrometer at 500 MHz and 125 MHz, respectively, or a Varian Mercury 300 spectrometer at 300 or 75 MHz, respectively. ¹³C spectra are referenced to residual CDCl₃ (77.2). ¹⁹F NMR spectra were recorded on a Varian 300 (at 282 MHz) and are reported relative to CFCl₃ (δ 0.0). Data for ¹H and ¹⁹F NMR spectra are reported as follows: chemical shift (δ ppm) (multiplicity, coupling constant (Hz), integration). MS were acquired using an Agilent 6200 Series TOF with an Agilent G1978A Multimode source in electrospray ionization (ESI), atmospheric pressure chemical ionization (APCI) or mixed (MM) ionization mode. Some compounds were synthesized in this work and others were obtained from the in-house compound library.

4.1.2 Synthesis of β-Nitro styrenes

β-Nitro styrenes were prepared according to a literature procedure [57] with minor modifications. See below for a representative procedure.



Scheme 1 Synthesis of compound **8**

E-1,2-dimethoxy-4-(2-nitrovinyl)benzene (**8**). A round-bottom flask fitted with a magnetic stir bar and a reflux condenser was flame-dried under vacuum. After cooling to ambient temperature under dry nitrogen, 3,4-dimethoxybenzaldehyde (0.419 g, 2.5 mmol, 1.0 equiv), ammonium acetate (0.170 g, 2.2 mmol, 0.9 equiv), and nitromethane (12.5 mL) were added, and the resulting mixture was heated to reflux and maintained with stirring for 14 hours. The reaction mixture was concentrated under reduced pressure, and the residue was recrystallized from ethanol to yield (**8**) (0.362 g, 69% yield) as yellow-green flakes: ¹H NMR (300 MHz, CDCl₃) δ 7.97 (d, *J* = 13.5 Hz, 1 H), 7.53 (d, *J* = 13.5 Hz, 1 H), 7.18 (dd, *J* = 8.7, 2.1 Hz, 1 H), 7.01 (d, *J* = 2.1 Hz, 1 H), 6.92 (d, *J* = 8.7 Hz, 1 H), 3.94 (s, 3 H) 3.93 (s, 3 H); MS (EI+) *m/z* 210.0 (M + H)⁺.

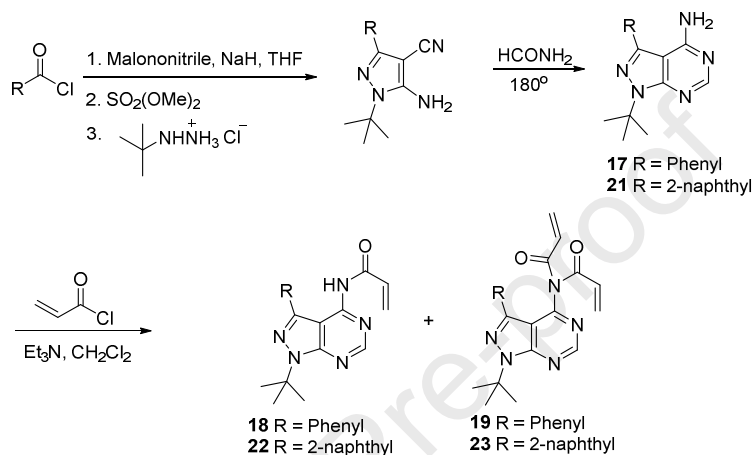
E-3-(2-nitrovinyl)pyridine (**13**). Prepared by the above procedure (3-pyridylcarboxaldehyde, 0.25 mL, 2.7 mmol). Purified by filtration through a short plug (SiO₂, 50% EtOAc in hexanes) followed by recrystallization from ethanol to yield (**13**) (0.112 g, 28% yield) as orange needles: ¹H NMR (300 MHz, CDCl₃) δ 8.80 (d, *J* = 2.1 Hz, 1 H), 8.72 (d, *J* = 4.8, 1.5 Hz, 1 H), 8.01 (d, *J* = 13.8 Hz, 1 H), 7.87 (ddd, *J* = 7.8, 2.1, 1.5 Hz, 1 H), 7.62 (d, *J* = 13.5 Hz, 1 H), 7.41 (dd, *J* = 7.8, 4.8 Hz, 1 H); HRMS (MM: ESI-APCI) calc'd for C₇H₇N₂O₂ [M + H]⁺: 151.0502, found 151.0503.

E-1-nitro-3-(2-nitrovinyl)benzene (**14**). Prepared by the above procedure (3-nitrobenzaldehyde, 0.389 g). Purified by flash chromatography (SiO₂, 17% EtOAc in hexane), followed by recrystallization from ethanol to yield (**14**) (0.228 g, 46% yield) as pale yellow powder: ¹H NMR (300 MHz, CDCl₃) δ 8.42 (t, *J* = 1.8 Hz, 1 H), 8.35 (ddd, *J* = 8.1, 1.8, 1.2 Hz, 1 H), 8.05 (d, *J* = 13.5 Hz, 1 H), 7.87 (dt, *J* = 7.5, 1.2 Hz, 1 H), 7.68 (t, *J* = 7.8 Hz, 1 H) 7.66 (d, *J* = 13.8 Hz, 1 H).

E-pentafluoro(2-nitrovinyl)benzene (**15**). Prepared by the above procedure (pentafluoro benzaldehyde, 0.538 g, 2.7 mmol). Purified by filtration through a short plug (SiO₂, 50% EtOAc in hexanes) followed by flash chromatography (SiO₂, 10% EtOAc in hexanes) to yield (**15**) (0.142 g, 22% yield) as yellow oil: ¹H NMR (300 MHz, CDCl₃) δ 8.04 (d, *J* = 13.8 Hz, 1 H), 7.82 (d, *J* = 13.8 Hz, 1 H); ¹⁹F NMR (282 MHz, CDCl₃) δ 135.8 (m, 2 F), 146.6 (tt, *J* = 20.7, 4.6 Hz, 1 F), 159.7 (m, 2 F).

E-2-bromo-1-fluoro-4-(2-nitrovinyl)benzene (**16**). Prepared by the above procedure (3-bromo-4-fluorobenzaldehyde, 0.500 g, 2.5 mmol). Purified by filtration through a short plug (SiO₂, 50% EtOAc in hexanes) followed by recrystallization from ethanol to yield (**16**) (0.311 g, 51% yield) as yellow microcrystals: ¹H NMR (300 MHz, CDCl₃) δ 7.91 (d, *J* = 13.5 Hz, 1 H), 7.77 (dd, *J* = 6.6, 2.4 Hz, 1 H), 7.51 (d, *J* = 13.8 Hz, 1 H), 7.49 (m, 1 H), 7.21 (t, *J* = 8.4 Hz, 1 H); ¹³C NMR (125 MHz, CDCl₃) δ 161.1 (d, *J* = 255 Hz), 137.7 (d, *J* = 2.9 Hz), 136.4, 134.2, 129.9 (d, *J* = 10.6 Hz), 127.8 (d, *J* = 3.4 Hz), 117.6 (d, *J* = 22.9 Hz), 110.6 (d, *J* = 21.9 Hz); ¹⁹F NMR (282 MHz, CDCl₃) δ 100.3 (dd, *J* = 11.8, 7.1 Hz, 1 F).

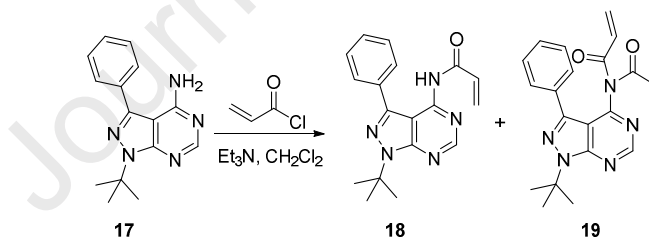
4.1.3 Synthesis of Pyrazolopyrimidine analogues



Scheme 2 Synthetic Route of Pyrazolopyrimidine analogues

Pyrazolopyrimidines **17**, **21**, and **26** were synthesized from the corresponding acid chloride [47, 58].

4.1.3.1 Synthesis of Compounds **18** and **19**



Scheme 3 Synthesis of compounds **18** and **19**

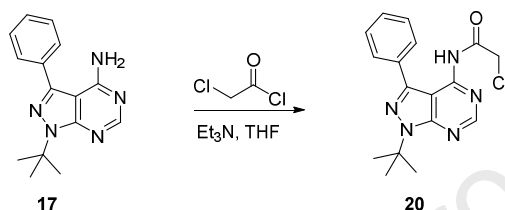
Representative Procedure for Acylation of Pyrazolopyrimidines: To a solution of 4-amino-1-*tert*-butyl-3-phenylpyrazolo[3,4-*d*] pyrimidine (**17**) (0.103 g, 0.387 mmol) in CH₂Cl₂ (4 mL, 0.1 M) was added Et₃N (0.043 mL, 0.31 mmol). The solution was cooled in an ice water bath, and acryloyl chloride (0.027 mL, 0.314 mmol) was added dropwise. After stirring for 30 minutes while warming to room temperature, the solution was partially concentrated and purified directly by silica gel column chromatography (10% ethyl acetate/hexanes). In addition to recovered starting material (0.0306 g, 0.1145 mmol, 29.6 % yield), three products were isolated:

N-(1-(*tert*-butyl)-3-phenyl-1*H*-pyrazolo[3,4-*d*]pyrimidin-4-yl)acrylamide (**18**) as white solid (0.015 g, 0.046 mmol, 14.5 % yield). ¹H NMR (300 MHz, *d*₆-DMSO): δ 11.04 (s, 1 H), 8.81 (s, 1 H), 7.61-7.56 (m, 2 H), 7.41-7.29 (m, 3 H), 6.37 (dd, *J* = 17.2, 10.2 Hz, 1 H), 5.86 (dd, *J* = 17.2, 1.6 Hz, 1 H), 5.65 (dd, *J* = 10.2, 1.6 Hz, 1 H), 1.82 (s, 9 H). HRMS (EI⁺) *m/z* calc'd for C₁₈H₁₉N₅O [M]⁺: 321.1590, found 321.1598. The ¹³C NMR data with good quality could not be obtained due to poor signal-to-noise as a result of a

peak broadening presumed to be a result of the dynamic process that was not investigated further due to the high reactivity of **18**.

N-acryloyl-*N*-(1-(*tert*-butyl)-3-phenyl-1*H*-pyrazolo[3,4-*d*]pyrimidin-4-yl)acrylamide (**19**) as white solid (0.019 g, 0.051 mmol, 16.2% yield). ¹H NMR (300 MHz, CDCl₃): δ 8.94 (s, 1 H), 7.50-7.45 (m, 2 H), 7.40-7.35 (m, 3 H), 6.31 (dd, *J* = 16.7, 2.3 Hz, 2 H), 6.22 (dd, *J* = 16.7, 9.3 Hz, 2 H), 5.63 (dd, *J* = 9.3, 2.3 Hz, 2 H), 1.9 (s, 9 H). ¹³C NMR (75 MHz, CDCl₃): δ 167.2, 155.4, 154.0, 153.5, 142.7, 132.1, 131.0, 129.8, 129.1, 129.0, 128.9, 110.2, 61.4, 29.3. HRMS (EI⁺) *m/z* calc'd for C₂₁H₂₁N₅O₂ [M]⁺: 375.1695, found 375.1695.

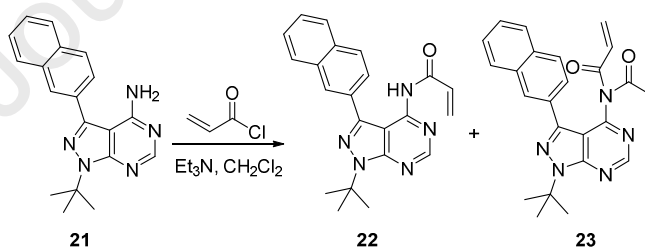
4.1.3.2 Synthesis of compound **20**



Scheme 4 Synthesis of compound **20**

To a THF (10 mL, 0.1 M) solution of phenyl pyrazolopyrimidine (**17**) (0.25 g, 0.94 mmol) was Et₃N (0.17 mL, 1.2 mmol). Chloroacetyl chloride (0.1 mL, 1.2 mmol) was added dropwise. After 12 hr at ambient temperature, the mixture was quenched with H₂O (10 mL) and extracted with CHCl₃ (3x10 mL). The combined organic layers were dried with MgSO₄, filtered, and concentrated. The crude oil was purified by silica gel column chromatography (1:1 hexanes/ethyl acetate) to provide **20** as white solid (0.18 g, 56 % yield). ¹H NMR (300 MHz, CDCl₃): δ 8.65 (br s, 2 H), 7.69 (br s, 2 H), 7.56-7.42 (m, 3 H), 4.37 (s, 2 H), 1.84 (s, 9 H). Many of the peaks in the ¹³C NMR spectrum were broadened by a dynamic process that was not investigated further. Poor signal-to-noise prevented acquisition of good ¹³C NMR spectral data. HRMS (FAB⁺) *m/z* calc'd for C₁₇H₁₉ON₅Cl [M + H]: 344.1273, found 344.1270.

4.1.3.3 Synthesis of compounds **22** and **23**



Scheme 5 Synthesis of compounds **22** and **23**

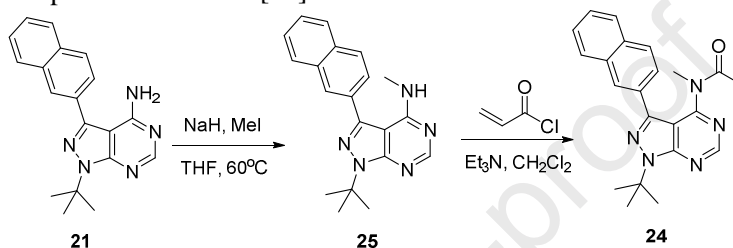
2-Naphthyl pyrazolopyrimidine (**21**) (0.1134 g, 0.357 mmol) was acylated as described in the above representative procedure using CH₂Cl₂ (3 mL), Et₃N (0.1 mL, 0.72 mmol) and acryloyl chloride (0.05 mL, 0.547 mmol). Water (10 mL) and NaHCO₃ (10 mL, saturated, aq.) were added and extracted with CH₂Cl₂ (3 x 10 mL). The combined organic layers were dried with Na₂SO₄, filtered, and concentrated under reduced pressure. The crude yellow oil was purified by silica column chromatography (1:9->1:3->1:0 ethyl acetate/hexanes) to provide three products in addition to recovered starting material (0.0184 g, 0.0466 mmol, 13% yield).

N-(1-(*tert*-butyl)-3-(naphthalen-2-yl)-1*H*-pyrazolo[3,4-*d*]pyrimidin-4-yl)acrylamide (**22**) as white solid (0.026 g, 0.069 mmol, 19 % Yield). ¹H NMR (300 MHz, DMSO) δ 11.23 (br s, 1 H), 8.82 (s, 1 H), 8.20 (s, 1 H), 7.91 (m, 3 H), 7.82 (d, *J* = 8 Hz, 1 H), 7.50 (m, 2 H), 6.32 (dd, *J* = 10, 17 Hz, 1 H), 5.73 (d, *J* = 17 Hz, 1 H), 5.51 (d, *J* = 10 Hz, 1 H), 1.86 (s, 9 H). Many of the peaks in the ¹³C NMR spectrum were

broadened by a dynamic process that was not investigated further. Poor signal-to-noise prevented acquisition of good ^{13}C NMR spectral data. HRMS (FAB+) m/z calc'd for $\text{C}_{22}\text{H}_{22}\text{N}_5\text{O}$ [M + H]: 372.1819; found 372.1811.

N-acryloyl-*N*-(1-(*tert*-butyl)-3-(naphthalen-2-yl)-1*H*-pyrazolo[3,4-*d*]pyrimidin-4-yl)acrylamide (**23**) as white solid (0.066 g, 0.16 mmol, 43 % Yield). ^1H NMR (500 MHz, CDCl_3) δ 8.94 (s, 1 H), 7.92 (s, 1 H), 7.84 (d, $J = 8.4$ Hz, 1 H), 7.81 (m, 1 H), 7.76 (m, 1 H), 7.61 (dd, $J = 8.4, 1.2$ Hz, 1 H), 7.48 (m, 2 H), 6.18 (ABX quartet, 4 H), 5.46 (dd, $J = 9.1, 2.8$ Hz, 2 H), 1.9 (s, 9 H). ^{13}C NMR (125 MHz, CDCl_3) δ 167.3, 155.6, 154.1, 153.6, 142.7, 133.5, 133.4, 131.1, 129.7, 129.5, 128.8, 128.7, 128.4, 127.9, 126.9, 126.8, 126.4, 110.3, 61.8, 29.5. HRMS (FAB+) m/z calc'd for $\text{C}_{25}\text{H}_{24}\text{N}_5\text{O}_2$ [M + H]: 426.1925; found 426.1930.

4.1.3.4 Synthesis of compounds **24** and **25** [59]

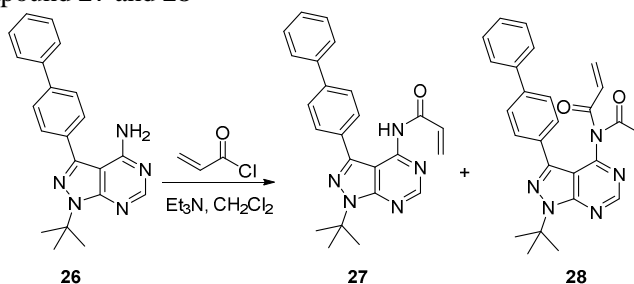


Scheme 6 Synthesis of compounds **24** and **25**

To solution of NaH (0.0055 g, 0.1375 mmol, 1.4 equiv.) and pyrazolopyrimidine **21** (0.0277 g, 0.1 mmol) in THF (3 mL, 0.03 M) was added CH_3I (0.006 mL, 0.096 mmol). The solution was heated to 60 °C for 5 hr. The solution was purified without workup by silica gel column chromatography (5% ethyl acetate / hexanes) to yield the monomethylated pyrazolopyrimidine (**25**) as white solid (0.0277 g, 0.0836 mmol, 87% yield). ^1H NMR (500 MHz, CDCl_3): δ 8.47 (s, 1 H), 8.11 (s, 1 H), 8.01 (d, $J = 8.4$ Hz, 1 H), 7.93 (m, 2 H), 7.78 (dd, $J = 8.4, 1.6$ Hz, 1 H), 7.56 (m, 2 H), 5.36 (br s, 1 H), 3.05 (d, $J = 4.9$ Hz, 3 H), 1.86 (s, 9 H). ^{13}C NMR (125 MHz, CDCl_3): δ 158.0, 154.8, 153.9, 141.7, 133.7, 133.4, 131.7, 129.4, 128.4, 128.1, 128.0, 127.0, 126.9, 126.4, 100.4, 60.6, 29.4, 28.0. HRMS (FAB+) m/z calc'd for $\text{C}_{20}\text{H}_{22}\text{N}_5$ [M + H]: 332.1870; found 332.1885.

To a solution of methylated pyrazolopyrimidine **25** (0.0277 g, 0.0836 mmol) in CH_2Cl_2 (5 mL, 0.02 M) was added Et_3N (0.022 mL, 0.16 mmol). The solution was cooled in an ice water bath and to it added acryloyl chloride (0.012 mL, 0.14 mmol). The solution was purified without workup by silica gel column chromatography (5% ethyl acetate/ benzene) to yield **24** as colorless oil (0.0015 g, 0.0039 mmol, 4.7% yield) along with recovered starting material (0.017 g, 62.4%). ^1H NMR (500 MHz, CDCl_3): δ 8.88 (s, 1 H), 8.05 (d, $J = 1.6$ Hz, 1 H), 7.91 (d, $J = 8.5$ Hz, 1 H), 7.86 (m, 2 H), 7.74 (dd, $J = 8.5, 1.8$ Hz, 1 H), 7.52 (m, 2 H), 6.20 (dd, $J = 10.1, 1.9$ Hz, 1 H), 6.10 (dd, $J = 16.7, 1.9$ Hz, 1 H), 5.46 (dd, $J = 16.7, 10.1$ Hz, 1 H), 3.20 (s, 3 H), 1.93 (s, 9 H). ^{13}C NMR (500 MHz, CDCl_3): δ 166.4, 157.7, 155.9, 153.8, 142.6, 133.5, 133.5, 130.0, 128.8, 128.8, 128.7, 128.7, 128.3, 128.0, 127.0, 126.9, 125.9, 108.4, 61.7, 36.3, 29.4. HRMS (FAB+) m/z calc'd for $\text{C}_{23}\text{H}_{24}\text{N}_5\text{O}$ [M + H]: 386.1975; found 386.1969.

4.1.3.5 Synthesis of compound **27** and **28**



Scheme 7 Synthesis of compound **27** and **28**

Biphenyl pyrazolopyrimidine (**26**) (0.2 g, 0.58 mmol) was acylated as described in the above representative procedure using CH₂Cl₂ (10 mL, 0.06 M), Et₃N (0.104 mL, 0.75 mmol), and acryloyl chloride (0.04 mL, 0.44 mmol). Purification by silica gel column chromatography (1:3 ethyl acetate/hexanes) yielded two products in addition to recovered starting material (0.042 g, 0.12 mmol, 21% yield). Data for starting pyrazolopyrimidine (**26**): ¹H NMR (300 MHz, CDCl₃): δ 8.37 (s, 1 H), 7.77 (m, 4 H), 7.65 (m, 2 H), 7.48 (m, 2 H), 7.39 (m, 1 H), 5.68 (br s, 2 H), 1.85 (s, 9 H). ¹³C NMR (125 MHz, CDCl₃): δ 158.0, 154.7, 154.5, 141.9, 141.8, 140.6, 132.8, 129.2, 129.1, 128.2, 127.9, 127.3, 100.0, 60.7, 29.4. HRMS (FAB+) *m/z* calc'd for C₂₁H₂₂N₅ [M + H]: 344.1870; found 344.1866.

N-(3-([1,1'-biphenyl]-4-yl)-1-(*tert*-butyl)-1*H*-pyrazolo[3,4-*d*]pyrimidin-4-yl)acrylamide (**27**) as white solid (0.022 g, 0.055 mmol, 9.5% yield). ¹H NMR (300 MHz, *d*₆-DMSO): δ 11.10 (br s, 1 H), 8.80 (s, 1 H), 7.68 (br m, 6 H), 7.48 (m, 2 H), 7.37 (m, 1 H), 6.4 (dd, *J* = 17.1, 10.3 Hz, 1 H), 5.89 (d, *J* = 17.1 Hz, 1 H), 5.66 (dd, *J* = 10.3, 1.6 Hz, 1 H), 1.83 (s, 9 H). Many of the peaks in the ¹³C NMR spectrum were broadened by a dynamic process that was not investigated further. Poor signal-to-noise prevented acquisition of good ¹³C NMR spectral data. HRMS (FAB+) *m/z* calc'd. for C₂₄H₂₄N₅O [M + H]: 398.1975; found 398.1962.

N-(3-([1,1'-biphenyl]-4-yl)-1-(*tert*-butyl)-1*H*-pyrazolo[3,4-*d*]pyrimidin-4-yl)-*N*-acryloylacrylamide (**28**) as white solid (0.030 g, 0.066 mmol, 11.5% yield). ¹H NMR (300 MHz, CDCl₃) δ 8.95 (s, 1 H), 7.54-7.64 (m, 6 H), 7.47 (m, 2 H), 7.38 (m, 1 H), 6.3 (ABX quartet, *J*_{AB} = 16.6 Hz, *J*_{AX} = 3.2 Hz, *J*_{BX} = 8.5 Hz, 4 H), 5.63 (dd, *J* = 8.5, 3.2 Hz, 2 H), 1.91 (s, 9 H). ¹³C NMR (125 MHz, CDCl₃) δ 167.23, 155.4, 154.0, 153.5, 142.4, 141.9, 140.7, 131.0, 131.0, 129.8, 129.5, 129.1, 127.8, 127.6, 127.3, 110.1, 61.8, 29.5.

4.2. Protein purification

Plasmids and primers used in this study are listed in Table S1. Proteins were purified as previously described [21, 41]. *E. coli* BL21 (DE3) containing the plasmid was grown in LB medium containing 50 µg/L ampicillin, which was shaken at 37 °C to an OD₆₀₀ of 0.5. The cell culture was cooled down to 22 °C and induced with 1 mM isopropyl-beta-D-thiogalactopyranoside (IPTG) and harvested 8–10 h later by centrifugation. The cell pellet (≈6 g from 2 L) was suspended in the 30 mL lysis buffer [100 mM Tris (pH 7.4), 500 mM KCl, 5 mM MgCl₂, 20 mM imidazole, 5% glycerol, 2 mM β-mercaptoethanol, and protease inhibitor tablet (Roche)]. The cells (held in an ice bath) were lysed by six 30-s pulses of sonication, separated by 2-min intervals. The lysate was centrifuged at 20,000 × *g* for 45 min at 4 °C, and the resulting supernatant was loaded onto a Ni-NTA column [5-mL suspension, preequilibrated with wash buffer (50 mL, 50 mM HEPES [pH 7.4], 150 mM KCl, 5 mM MgCl₂, and 20 mM imidazole)] and incubated at 4 °C with rotation for 30 min. The column was then flushed with wash buffer (100 mL), and His6-tagged p97 was eluted by stepwise application of 10 mL of imidazole elution buffer (50 mM, 100 mM, 150 mM, 200 mM, or 250 mM imidazole in wash buffer). Fractions from the 200-mM and 250-mM imidazole steps were combined and concentrated with an Amicon Ultra-15 centrifugal filter unit (nominal molecular weight limit = 100 kDa). The mixture (0.5 mL of 20 mg/mL) was then fractionated with a gel filtration column (Tricorn Superdex 200; GE Healthcare), eluted with GF buffer [20 mM HEPES (pH 7.4), 250 mM KCl, and 1 mM MgCl₂] at 0.5 mL/min flow rate, and fractions corresponding to an apparent molecular weight of 500–600 kDa were collected and analyzed by 4–12% SDS/PAGE to evaluate purity (Invitrogen). Fractions that contained p97 of ≥95% purity were concentrated to 5 mg/mL, exchanged into storage buffer [20 mM HEPES (pH 7.4), 250 mM KCl, 1 mM MgCl₂, 5% glycerol, and 1 mM DTT], aliquoted, frozen in liquid nitrogen, and stored at –80 °C.

4.3. ATPase activity

The purified protein was assayed in 50 µL ATPase assay buffer (50 mM Tris pH 7.4, 20 mM MgCl₂, 1mM EDTA, 0.5 mM TCEP, and 0.01% Triton X-100) containing 200 µM ATP. After a 60 min-incubation at room temperature, 50 µL Biomol Green reagent (Enzo Life Sciences) was added to stop the

reaction, and the absorbance at 635 nm was measured using a BioTek Synergy Neo 2 plate reader. The eight-dose titrations were performed of the compound to the reaction to determine the IC₅₀ values of the compounds. The results were calculated from six replicates using GraphPad Prism 7.0.

4.4. Ub^{G76V}-GFP and ODD-Luc degradation

This assay was described previously [41]. Ub^{G76V}-GFP/ODD-Luc HeLa cells were seeded as 5000 cells per well per 30 μ L in 384 well plate (Greiner 781091). Clear DMEM containing 2.5% FBS, 1% L-Glutamine, and 1% Penicillin-Streptomycin (Thermo Fisher) was used as an assay medium. The 4 μ M of MG132 (50 μ L of 4 mM MG132 into 50 mL pre-warmed clear DMEM) was prepared, added into each well (25 μ L), and incubated at 37°C for 60 min. Each well was washed with 100 μ L PBS twice using a Biotek MultiFlo Microplate dispenser and 30 μ L CHX/clear DMEM solution (50 μ L of 50 mM cycloheximide into 50 mL pre-warmed clear DMEM) was added. 10 μ L of compound was added and incubated for 120 min at 37°C. Then each well was washed with 100 μ L PBS, and 20 μ L of assay medium was dispensed per well. ImageXpress High Content Confocal Screening System was used to read the GFP signal. Next, 10 μ L D-luciferin (2.5 mg/mL in PBS) was added, shaken for 5 sec, and incubated at r.t. for 10 min. Synergy NEO multi-mode microplate reader was used to read the Luciferase signal. Data was calculated from quadruplicate to obtain the IC₅₀ using GraphPad Prism 7.0.

4.5 Human 26S Proteasome Activity Assay

Human 26S proteasome complex was affinity purified from HEK293 cells that stably express tagged human Rpn 11, as described [50]. Purified human 26S proteasome (19 nM) was incubated with 5, 25, or 50 μ M of MG132 or PPA in assay buffer [50 mM Tris (pH 7.4), 20 mM MgCl₂, 1 mM EDTA, 0.5 mM TCEP, and 100 μ M ATP] for 30 min at room temperature and the fluorogenic proteasome substrate (succinyl-Leu-Leu-Val-Tyr-AMC, 60 μ M; Boston Biochem) was added to initiate the reaction. Fluorescence intensity was monitored every 3 min over 30 min. IC₅₀ values of the compounds were calculated from sextuplicate using GraphPad Prism 7.0.

4.6. Western blot

TCR α -GFP (α -chain of the T-cell receptor fused to GFP) 293 cells were treated with 4 μ M MG132 for 1 h, washed, and then incubated in the presence of 50 μ M cycloheximide plus 10 μ M test compound or MG132 (as a positive control) for 60 min or 120 min prior to harvest. Samples were immunoblotted to detect p97, and TCR α -GFP. The level of p97 served as a loading control. Primary antibodies used were anti-p97 (MA3-004, Thermo Scientific), and anti-GFP (Y1030, 2BSscientific), ECL reagent (WBKLS0500, MilliporeSigma) and ChemiDoc MP Imaging System (Bio-Rad) was used to image the blots.

4.7. Docking study

The structure of PPA was prepared using Chem3D by CambridgeSoft. The geometry and energy of the structure were optimized using MM2 force field. AutoDock 4.2 was used to identify the binding mode of PPA responsible for the activity. The receptor WT-p97 in PDB format (PDB code: 5FTK) was obtained from the RCSB protein data bank (<https://www.rcsb.org/>), which was treated by the removal of water and the addition of hydrogen. The docking results were visualized using Ligplot⁺ [60] and PyMol (version 0.99; Delano Scientific, San Carlos, CA, USA).

4.8. Anti-proliferative assay

Anti-proliferative activity was measured using the CellTiter Glo[®] Luminescent Cell Viability Assay (Promega G7572) according to the manufacturer's procedure. RPMI1640 or DMEM containing 5% FBS and 1% Penicillin-Streptomycin was used as the cell viability assay medium. To find the linear relationship between the relative luminescence unit and the number of viable cells, a standard curve for each cell line was generated. Generally, 30 μ L of cell suspension was plated in 384-well plates (Greiner 781080) with serial 2-fold dilutions (from 30000 to 284 cells per well). Twenty-four hours after seeding,

8 μ L of assay media containing 5% DMSO was added into each well, and the plates were incubated for an additional 48 hr at 37 °C in a 5% CO₂ incubator. To test the anti-proliferative activity of p97 inhibitors, cells were seeded at 750 or 3000 cells per well according to the linear range determined from the standard curve of each cell line. Twenty-four hours after seeding, cells were treated with the compounds (three-fold dilution, eight concentrations). After 48 hours of treatment, cell viability was measured by CellTiter Glo, and IC₅₀ values were calculated using the percentage of growth of treated cells versus the DMSO control. The results were analyzed using GraphPad Prism 7.0.

4.9. Proteomics

HCT116 cells were treated with DMSO, 15 μ M or 30 μ M PPA for 6 h, and pellets were harvested. The LC-MS samples were prepared by following the instructions of Thermo EasyPep Mini MS Sample Prep Kit (REF A4006) and peptide concentration was tested through Pierce Quantitative Fluorometric Peptide Assay (cat# 23290).

The LC-MS/MS experiments were performed using an EASY-nLC 1000 (ThermoFisher Scientific, San Jose, CA) connected to an Orbitrap Eclipse Tribrid mass spectrometer (Thermo Fisher Scientific, San Jose, CA). The sample (1 μ g) in 0.1% FA solution was loaded onto an Aurora UHPLC Column (25 cm x 75 μ m, 1.6 μ m C18, AUR2-25075C18A, Ion Opticks) and separated over 136 min at a flow rate of 0.35 μ L/min with the following gradient: 2-6% Solvent B (7.5 min), 6-25% B (82.5 min), 25-40% B (30 min), 40-98% B (1 min), and 98% B (15 min). Solvent A consisted of 97.9% H₂O, 2% ACN, and 0.1% formic acid, and solvent B consisted of 19.9% H₂O, 80% ACN, and 0.1% formic acid. An MS1 scan was acquired in the Orbitrap at 120,000 resolution with a scan range of 350-1500 m/z. The AGC target was 4×10^5 , and the maximum injection time was 50 mins. Dynamic exclusion was set to exclude features after 1 time for 60 s with a 10-ppm mass tolerance. Higher-energy collisional dissociation (HCD) fragmentation was performed with 35% collision energy after quadruple isolation of features using a 1.6 m/z isolation window, 5×10^4 AGC target, and 35 ms maximum injection time. MS2 scans were then also acquired by the Orbitrap with 50,000 resolution. Ion source settings were as follows: ion source type, NSI; spray voltage, 2400 V; ion transfer tube temperature, 275 °C. System control and data collection were performed by Xcalibur software.

The proteomic analysis was performed through Proteome Discoverer 2.4 (Thermo Scientific) using the Uniprot human database and the Byonic search algorithm (Protein Metrics). Percolator FDRs were set at 0.001 (strict) and 0.01 (relaxed). Peptide FDRs were set at 0.001 (strict) and 0.01 (relaxed), with medium confidence and a minimum peptide length of 6. Normalization was performed on the total peptide amount. The limma analysis was performed using R studio following the user guide [61]. The volcano figures were plotted by GraphPad Prism 7.0. The Venn diagram was performed using FunRich 3.1. The heatmap figure was plotted by heatmapper (<http://www.heatmapper.ca/>). The gene ontology analysis was performed by DAVID 6.8 (<https://david-d.ncifcrf.gov/>). [62] The enrichment dot bubble figure was plotted by <http://www.bioinformatics.com.cn>. And the protein-protein interaction analysis was performed using the STRING database (<http://www.stringdb.org/>). [63]

Declaration of competing interest

The authors have no conflicts of interest to declare.

Acknowledgments

We thank M. S. Cohen, J. Taunton, and K. Shokat for providing compounds 4,5,6, M. Smythe and C. Crews for YU101, A. M. Weissman for PYR-41, C. C. Wu for β -nitrostyrene analogues (compounds 7, 9,10,11,12), Y. Ye at NIDDK/NIH for providing yeast Cdc48 and hamster NSF plasmids. A.C.J. was supported by NIH Grant F32GM082000; A.F.G.G thanks the Natural Sciences and Engineering Research Council (NSERC) of Canada for a PGS D scholarship; R.J.D. was an HHMI Investigator, and this work was funded in part by HHMI; This work was funded in part by the NIH-NINDS (R01NS100815) to

T.F.C. and NIH-NIGMS (R01GM080269) to B.M.S. We thank the anonymous reviewers for constructive criticism.

Author contributions

Gang Zhang wrote the manuscript and analyzed the potential interaction between PPA and p97 by molecular docking. Shan Li and Feng Wang performed the anti-proliferative assay and proteomics study. Amanda C. Jones, Alexander F. G. Goldberg, and Scott Virgil synthesized and characterized the target compounds. Tsui-Fen Chou performed experiments in tables 1-4; Figures 2 and 4. Amanda C. Jones, Brian M. Stoltz, Raymond J. Deshaies, and Tsui-Fen Chou conceived the project and made the major contribution in the design of the initial work.

Conflicts of interest

The authors have no conflicts of interest to declare.

Appendix A. Supporting information

Supporting data to this article can be found online at <https://doi.org/xx.xxxx/xxxxxxxxxxxxx>.

References

- [1] F. Confalonieri, M. Duguet, A 200-amino acid ATPase module in search of a basic function, *Bioessays*, 17 (1995) 639-650.
- [2] N.A. Ranson, H.E. White, H.R. Saibil, Chaperonins, *Biochem. J.*, 333 (Pt 2) (1998) 233-242.
- [3] N. Hirokawa, Y. Noda, Y. Okada, Kinesin and dynein superfamily proteins in organelle transport and cell division, *Curr. Opin. Cell Biol.*, 10 (1998) 60-73.
- [4] T. Langer, AAA proteases: cellular machines for degrading membrane proteins, *Trends Biochem. Sci.*, 25 (2000) 247-251.
- [5] D.G. Lee, S.P. Bell, ATPase switches controlling DNA replication initiation, *Curr. Opin. Cell Biol.*, 12 (2000) 280-285.
- [6] W. Yang, Structure and function of mismatch repair proteins, *Mutat. Res.*, 460 (2000) 245-256.
- [7] J.M. Caruthers, D.B. McKay, Helicase structure and mechanism, *Curr. Opin. Struct. Biol.*, 12 (2002) 123-133.
- [8] T. Nishi, M. Forgac, The vacuolar (H⁺)-ATPases--nature's most versatile proton pumps, *Nat. Rev. Mol. Cell Biol.*, 3 (2002) 94-103.
- [9] X. Zhang, A. Shaw, P.A. Bates, R.H. Newman, B. Gowen, E. Orlova, M.A. Gorman, H. Kondo, P. Dokurno, J. Lally, G. Leonard, H. Meyer, M. van Heel, P.S. Freemont, Structure of the AAA ATPase p97, *Mol. Cell*, 6 (2000) 1473-1484.
- [10] A. Buchberger, H. Schindelin, P. Hanzelmann, Control of p97 function by cofactor binding, *FEBS Lett.*, 589 (2015) 2578-2589.
- [11] T. Ogura, A.J. Wilkinson, AAA+ superfamily ATPases: common structure--diverse function, *Genes Cells*, 6 (2001) 575-597.
- [12] Q. Wang, C. Song, X. Yang, C.C. Li, D1 ring is stable and nucleotide-independent, whereas D2 ring undergoes major conformational changes during the ATPase cycle of p97-VCP, *J. Biol. Chem.*, 278 (2003) 32784-32793.
- [13] C. Song, Q. Wang, C.C. Li, ATPase activity of p97-valosin-containing protein (VCP). D2 mediates the major enzyme activity, and D1 contributes to the heat-induced activity, *J. Biol. Chem.*, 278 (2003) 3648-3655.

- [14] Y. Ye, H.H. Meyer, T.A. Rapoport, Function of the p97-Ufd1-Npl4 complex in retrotranslocation from the ER to the cytosol: dual recognition of nonubiquitinated polypeptide segments and polyubiquitin chains, *J. Cell Biol.*, 162 (2003) 71-84.
- [15] H.W. Platta, M.O. Debelyy, F.E. Magraoui, R. Erdmann, The AAA peroxins Pex1p and Pex6p function as dislocases for the ubiquitinated peroxisomal import receptor Pex5p, *Biochem. Soc. Trans.*, 36 (2008) 99-104.
- [16] H.W. Platta, S. Grunau, K. Rosenkranz, W. Girzalsky, R. Erdmann, Functional role of the AAA peroxins in dislocation of the cycling PTS1 receptor back to the cytosol, *Nat. Cell Biol.*, 7 (2005) 817-822.
- [17] M. Bug, H. Meyer, Expanding into new markets--VCP/p97 in endocytosis and autophagy, *J. Struct. Biol.*, 179 (2012) 78-82.
- [18] D. Fessart, E. Marza, S. Taouji, F. Delom, E. Chevet, P97/CDC-48: proteostasis control in tumor cell biology, *Cancer Lett.*, 337 (2013) 26-34.
- [19] N. Nishimura, M.O. Radwan, M. Amano, S. Endo, E. Fujii, H. Hayashi, S. Ueno, N. Ueno, H. Tatetsu, H. Hata, Y. Okamoto, M. Otsuka, H. Mitsuya, M. Matsuoka, Y. Okuno, Novel p97/VCP inhibitor induces endoplasmic reticulum stress and apoptosis in both bortezomib-sensitive and -resistant multiple myeloma cells, *Cancer Sci.*, 110 (2019) 3275-3287.
- [20] C.J. Fang, L. Gui, X. Zhang, D.R. Moen, K. Li, K.J. Frankowski, H.J. Lin, F.J. Schoenen, T.F. Chou, Evaluating p97 inhibitor analogues for their domain selectivity and potency against the p97-p47 complex, *ChemMedChem*, 10 (2015) 52-56.
- [21] T.F. Chou, S.J. Brown, D. Minond, B.E. Nordin, K. Li, A.C. Jones, P. Chase, P.R. Porubsky, B.M. Stoltz, F.J. Schoenen, M.P. Patricelli, P. Hodder, H. Rosen, R.J. Deshaies, Reversible inhibitor of p97, DBE-Q, impairs both ubiquitin-dependent and autophagic protein clearance pathways, *Proc. Natl. Acad. Sci. U.S.A.*, 108 (2011) 4834-4839.
- [22] T.F. Chou, K. Li, K.J. Frankowski, F.J. Schoenen, R.J. Deshaies, Structure-activity relationship study reveals ML240 and ML241 as potent and selective inhibitors of p97 ATPase, *ChemMedChem*, 8 (2013) 297-312.
- [23] D.J. Anderson, R.L. Moigne, S. Djakovic, B. Kumar, J. Rice, S. Wong, J. Wang, B. Yao, E. Valle, S. Kiss von Soly, A. Madriaga, F. Soriano, M.K. Menon, Z.Y. Wu, M. Kampmann, Y. Chen, J.S. Weissman, B.T. Aftab, F.M. Yakes, L. Shawver, H.J. Zhou, D. Wustrow, M. Rolfe, Targeting the AAA ATPase p97 as an Approach to Treat Cancer through Disruption of Protein Homeostasis, *Cancer Cell*, 28 (2015) 653-665.
- [24] F. Wang, S. Li, T. Gan, G.M. Stott, A. Flint, T.F. Chou, Allosteric p97 Inhibitors Can Overcome Resistance to ATP-Competitive p97 Inhibitors for Potential Anticancer Therapy, *ChemMedChem*, 15 (2020) 685-694.
- [25] ClinicalTrials, Study of CB-5339 in Acute Myeloid Leukemia or Myelodysplastic Syndrome, <https://clinicaltrials.gov/ct2/show/NCT04402541>, July 14 2020 .
- [26] R. Ding, T. Zhang, D.J. Wilson, J. Xie, J. Williams, Y. Xu, Y. Ye, L. Chen, Discovery of Irreversible p97 Inhibitors, *J. Med. Chem.*, 62 (2019) 2814-2829.
- [27] P. Polucci, P. Magnaghi, M. Angiolini, D. Asa, N. Avanzi, A. Badari, J. Bertrand, E. Casale, S. Cauteruccio, A. Cirila, L. Cozzi, A. Galvani, P.K. Jackson, Y. Liu, S. Magnuson, B. Malgesini, S. Nuvoloni, C. Orrenius, F.R. Sirtori, L. Riceputi, S. Rizzi, B. Trucchi, T. O'Brien, A. Isacchi, D. Donati, R. D'Alessio, Alkylsulfanyl-1,2,4-triazoles, a new class of allosteric valosine containing protein inhibitors. Synthesis and structure-activity relationships, *J. Med. Chem.*, 56 (2013) 437-450.

- [28] P. Magnaghi, R. D'Alessio, B. Valsasina, N. Avanzi, S. Rizzi, D. Asa, F. Gasparri, L. Cozzi, U. Cucchi, C. Orrenius, P. Polucci, D. Ballinari, C. Perrera, A. Leone, G. Cervi, E. Casale, Y. Xiao, C. Wong, D.J. Anderson, A. Galvani, D. Donati, T. O'Brien, P.K. Jackson, A. Isacchi, Covalent and allosteric inhibitors of the ATPase VCP/p97 induce cancer cell death, *Nat. Chem. Biol.*, 9 (2013) 548-556.
- [29] H. Luo, H. Song, R. Mao, Q. Gao, Z. Feng, N. Wang, S. Song, R. Jiao, P. Ni, H. Ge, Targeting valosin-containing protein enhances the efficacy of radiation therapy in esophageal squamous cell carcinoma, *Cancer Sci.*, 110 (2019) 3464-3475.
- [30] S. Banerjee, A. Bartesaghi, A. Merk, P. Rao, S.L. Bulfer, Y. Yan, N. Green, B. Mroczkowski, R.J. Neitz, P. Wipf, V. Falconieri, R.J. Deshaies, J.L. Milne, D. Huryn, M. Arkin, S. Subramaniam, 2.3 Å resolution cryo-EM structure of human p97 and mechanism of allosteric inhibition, *Science*, 351 (2016) 871-875.
- [31] Q. Wang, L. Li, Y. Ye, Inhibition of p97-dependent protein degradation by Eeyarestatin I, *J. Biol. Chem.*, 283 (2008) 7445-7454.
- [32] Q. Wang, B.A. Shinkre, J.G. Lee, M.A. Weniger, Y. Liu, W. Chen, A. Wiestner, W.C. Trenkle, Y. Ye, The ERAD inhibitor Eeyarestatin I is a bifunctional compound with a membrane-binding domain and a p97/VCP inhibitory group, *PLoS One*, 5 (2010) e15479.
- [33] R. Pohler, J.H. Krahn, J. van den Boom, G. Dobrynin, F. Kaschani, H.M. Eggenweiler, F.T. Zenke, M. Kaiser, H. Meyer, A Non-Competitive Inhibitor of VCP/p97 and VPS4 Reveals Conserved Allosteric Circuits in Type I and II AAA ATPases, *Angew. Chem. Int. Ed.*, 57 (2018) 1576-1580.
- [34] C. Alvarez, S.L. Bulfer, R. Chakrasali, M.S. Chimenti, R.J. Deshaies, N. Green, M. Kelly, M.G. LaPorte, T.S. Lewis, M. Liang, W.J. Moore, R.J. Neitz, V.A. Peshkov, M.A. Walters, F. Zhang, M.R. Arkin, P. Wipf, D.M. Huryn, Allosteric Indole Amide Inhibitors of p97: Identification of a Novel Probe of the Ubiquitin Pathway, *ACS Med. Chem. Lett.*, 7 (2016) 182-187.
- [35] J. Tillotson, B.P. Bashyal, M. Kang, T. Shi, F. De La Cruz, A.A. Gunatilaka, E. Chapman, Selective inhibition of p97 by chlorinated analogues of dehydrocurvularin, *Org. Biomol. Chem.*, 14 (2016) 5918-5921.
- [36] S. Tao, J. Tillotson, E.M.K. Wijeratne, Y.M. Xu, M. Kang, T. Wu, E.C. Lau, C. Mesa, D.J. Mason, R.V. Brown, J.J. Clair, A.A.L. Gunatilaka, D.D. Zhang, E. Chapman, Withaferin A Analogs That Target the AAA+ Chaperone p97, *ACS Chem. Biol.*, 10 (2015) 1916-1924.
- [37] A. Segura-Cabrera, R. Tripathi, X. Zhang, L. Gui, T.F. Chou, K. Komurov, A structure- and chemical genomics-based approach for repositioning of drugs against VCP/p97 ATPase, *Sci. Rep.*, 7 (2017) 44912.
- [38] E.M. Wijeratne, G.M. Gunaherath, V.M. Chapla, J. Tillotson, F. de la Cruz, M. Kang, J.M. U'Ren, A.R. Araujo, A.E. Arnold, E. Chapman, A.A. Gunatilaka, Oxaspirol B with p97 Inhibitory Activity and Other Oxaspirols from *Lecythophora* sp. FL1375 and FL1031, Endolichenic Fungi Inhabiting *Parmotrema tinctorum* and *Cladonia evansii*, *J. Nat. Prod.*, 79 (2016) 340-352.
- [39] M.A. Arai, S. Taguchi, K. Komatsuzaki, K. Uchiyama, A. Masuda, M. Sampei, M. Satoh, S. Kado, M. Ishibashi, Valosin-containing Protein is a Target of 5'-I Fuligocandin B and Enhances TRAIL Resistance in Cancer Cells, *ChemistryOpen*, 5 (2016) 574-579.
- [40] M. Noguchi, T. Takata, Y. Kimura, A. Manno, K. Murakami, M. Koike, H. Ohizumi, S. Hori, A. Kakizuka, ATPase activity of p97/valosin-containing protein is regulated by oxidative

- modification of the evolutionally conserved cysteine 522 residue in Walker A motif, *J. Biol. Chem.*, 280 (2005) 41332-41341.
- [41] T.F. Chou, R.J. Deshaies, Quantitative cell-based protein degradation assays to identify and classify drugs that target the ubiquitin-proteasome system, *J. Biol. Chem.*, 286 (2011) 16546-16554.
- [42] W.Y. Wang, P.W. Hsieh, Y.C. Wu, C.C. Wu, Synthesis and pharmacological evaluation of novel beta-nitrostyrene derivatives as tyrosine kinase inhibitors with potent antiplatelet activity, *Biochem. Pharmacol.*, 74 (2007) 601-611.
- [43] W.Y. Wang, Y.C. Wu, C.C. Wu, Prevention of platelet glycoprotein IIb/IIIa activation by 3,4-methylenedioxy-beta-nitrostyrene, a novel tyrosine kinase inhibitor, *Mol. Pharmacol.*, 70 (2006) 1380-1389.
- [44] M.S. Cohen, C. Zhang, K.M. Shokat, J. Taunton, Structural bioinformatics-based design of selective, irreversible kinase inhibitors, *Science*, 308 (2005) 1318-1321.
- [45] J.A. Blair, D. Rauh, C. Kung, C.H. Yun, Q.W. Fan, H. Rode, C. Zhang, M.J. Eck, W.A. Weiss, K.M. Shokat, Structure-guided development of affinity probes for tyrosine kinases using chemical genetics, *Nat. Chem. Biol.*, 3 (2007) 229-238.
- [46] B. DeLaBarre, A.T. Brunger, Complete structure of p97/valosin-containing protein reveals communication between nucleotide domains, *Nat. Struct. Biol.*, 10 (2003) 856-863.
- [47] A.C. Bishop, C.-y. Kung, K. Shah, L. Witucki, K.M. Shokat, Y. Liu, Generation of Monospecific Nanomolar Tyrosine Kinase Inhibitors via a Chemical Genetic Approach, *J. Am. Chem. Soc.*, 121 (1999) 627-631.
- [48] J.H. Hanke, J.P. Gardner, R.L. Dow, P.S. Changelian, W.H. Brissette, E.J. Weringer, B.A. Pollok, P.A. Connelly, Discovery of a novel, potent, and Src family-selective tyrosine kinase inhibitor. Study of Lck- and FynT-dependent T cell activation, *J. Biol. Chem.*, 271 (1996) 695-701.
- [49] G.M. Morris, R. Huey, W. Lindstrom, M.F. Sanner, R.K. Belew, D.S. Goodsell, A.J. Olson, AutoDock4 and AutoDockTools4: Automated docking with selective receptor flexibility, *J. Comput. Chem.*, 30 (2009) 2785-2791.
- [50] X. Wang, C.-F. Chen, P.R. Baker, P.-l. Chen, P. Kaiser, L. Huang, Mass Spectrometric Characterization of the Affinity-Purified Human 26S Proteasome Complex†, *Biochemistry*, 46 (2007) 3553-3565.
- [51] B. DeLaBarre, J.C. Christianson, R.R. Kopito, A.T. Brunger, Central pore residues mediate the p97/VCP activity required for ERAD, *Mol. Cell*, 22 (2006) 451-462.
- [52] M. Elofsson, U. Splittgerber, J. Myung, R. Mohan, C.M. Crews, Towards subunit-specific proteasome inhibitors: synthesis and evaluation of peptide α' , β' -epoxyketones, *Chem. Biol.*, 6 (1999) 811-822.
- [53] Y. Yang, J. Kitagaki, R.M. Dai, Y.C. Tsai, K.L. Lorick, R.L. Ludwig, S.A. Pierre, J.P. Jensen, I.V. Davydov, P. Oberoi, C.C. Li, J.H. Kenten, J.A. Beutler, K.H. Vousden, A.M. Weissman, Inhibitors of ubiquitin-activating enzyme (E1), a new class of potential cancer therapeutics, *Cancer Res.*, 67 (2007) 9472-9481.
- [54] N.G. Her, J.I. Toth, C.T. Ma, Y. Wei, K. Motamedchaboki, E. Sergienko, M.D. Petroski, p97 Composition Changes Caused by Allosteric Inhibition Are Suppressed by an On-Target Mechanism that Increases the Enzyme's ATPase Activity, *Cell Chem. Biol.*, 23 (2016) 517-528.
- [55] P. Sanchez-Martin, M. Komatsu, p62/SQSTM1 - steering the cell through health and disease, *J. Cell Sci.*, 131 (2018).

- [56] L.F. Bentson, V.A. Agbor, L.N. Agbor, A.C. Lopez, L.E. Nfonsam, S.S. Bornstein, M.A. Handel, C.C. Linder, New point mutation in Golga3 causes multiple defects in spermatogenesis, *Andrology*, 1 (2013) 440-450.
- [57] C.S. Dowd, K. Herrick-Davis, C. Egan, A. DuPre, C. Smith, M. Teitler, R.A. Glennon, 1-[4-(3-Phenylalkyl)phenyl]-2-aminopropanes as 5-HT_{2A} Partial Agonists, *J. Med. Chem.*, 43 (2000) 3074-3084.
- [58] U. Hanefeld, C.W. Rees, A.J.P. White, D.J. Williams, One-pot synthesis of tetrasubstituted pyrazoles—proof of regiochemistry, *J. Chem. Soc., Perkin Trans. 1*, (1996) 1545-1552.
- [59] G. Guillaumet, O.-I. Patriciu, C. Pillard, A.-L. Fînaru, I. Săndulescu, Synthesis of Nitro N,N'-Dipyridinylamines via Oxidative Nucleophilic Substitution of Hydrogen, *Synthesis*, 2007 (2007) 3868-3876.
- [60] R.A. Laskowski, M.B. Swindells, LigPlot+: multiple ligand-protein interaction diagrams for drug discovery, *J. Chem. Inf. Model.*, 51 (2011) 2778-2786.
- [61] G.K. Smyth, N.P. Thorne, J. Wettenhall, Limma: Linear Models for Microarray Data User's Guide. Software manual available from <http://www.bioconductor.org>, 2003.
- [62] W. Huang da, B.T. Sherman, X. Zheng, J. Yang, T. Imamichi, R. Stephens, R.A. Lempicki, Extracting biological meaning from large gene lists with DAVID, *Curr. Protoc. Bioinformatics*, Chapter 13 (2009) Unit 13 11.
- [63] D. Szklarczyk, A.L. Gable, D. Lyon, A. Junge, S. Wyder, J. Huerta-Cepas, M. Simonovic, N.T. Doncheva, J.H. Morris, P. Bork, L.J. Jensen, C.V. Mering, STRING v11: protein-protein association networks with increased coverage, supporting functional discovery in genome-wide experimental datasets, *Nucleic Acids Res.*, 47 (2019) D607-D613.

Highlights

- Designed covalent p97 ATPase inhibitors to target the D2 active site.
- Identified PPA as a selective p97 covalent inhibitor.
- PPA can block growth of CB-5083 and NMS-873 resistant cancer cells.
- Proteomic analysis revealed PPA-induced protein level changes.

Journal Pre-proof

1. Conflict of Interest

We wish to confirm that there are no known conflicts of interest associated with this publication and there has been no significant financial support for this work that could have influenced its outcome.

Journal Pre-proof